Modeling and Analysis of Energy Efficiency in Wireless Handset Transceiver Systems

By

Farhad Mahmood

Submitted to the Department of Electrical Engineering and Computer Science and the
Graduate Faculty of the University of Kansas
in partial fulfillment of the requirements for the degree of
Doctor of Philosophy

Erik Perrins, Chairperson

Lingjia Liu, Co-Chairperson

Committee members

Victor Frost

Shannon Blunt

Bozenna Pasik-Duncan

Date defended: April 16, 2019

The Dissertation Committee for Farhad Mahmood certifies
that this is the approved version of the following dissertation :

Modeling and Analysis of Energy Efficiency in Wireless Handset Transceiver Systems

Erik Perrins, Chairperson

Date approved: April 16, 2019

Abstract

As wireless communication devices are taking a significant part in our daily life, research steps toward making these devices even faster and smarter are accelerating rapidly. The main limiting factors are energy and power consumption. Many techniques are utilized to increase the battery's capacity (Ampere per Hour), but that comes with a cost of raising the safety concerns. The other way to increase the battery's life is to decrease the energy consumption of the devices. In this work, we analyze energy-efficient communications for wireless devices based on an advanced energy consumption model that takes into account a broad range of parameters. The developed model captures relationships between transmission power, transceiver distance, modulation order, channel fading, power amplifier (PA) effects, power control, multiple antennas, as well as other circuit components in the radio frequency (RF) transceiver. Based on the developed model, we are able to identify the optimal modulation order in terms of energy efficiency under different situations (e.g., different transceiver distance, different PA classes and efficiencies, different pulse shape, etc). Furthermore, we capture the impact of system level and network level parameters on the PA energy via peak to average ratio (PAR) and power control. We are also able to identify the impact of multiple antennas at the handset on the energy consumption and the transmitted bit rate for few and many antennas (conventional multiple-input-multiple-output (MIMO)

and massive MIMO) at the base station. This work provides an important framework for analyzing energy-efficient communications for different wireless systems ranging from cellular networks to wireless internet of things.

Acknowledgements

I would like to thank my wife, Zereen, for her love and encouragements. I would also like to thank my advisors, Dr. Erik Perrins and Dr. Lingjia Liu, for the excellent mentorship and advices they have given me over the years, and finally to thank all the people who supported me during my Ph.D. journey.

Contents

List of Figures

List of Tables

Chapter 1

Introduction

In the world of wireless communications, many technologies have been implemented to increase spectral efficiency. One of the essential remaining concerns of wireless communication systems is the high value of energy consumption. Reducing the energy consumption of base stations can decrease the operating cost of wireless communication systems, and reduce greenhouse gas emissions [1]. On top of that, reducing the energy consumption of wireless handsets can extend the battery life, and also mitigate the critical power amplifier (PA) packaging heat issues [2]. Increasing the density/capacity (measured in Ampere-hours) is an alternative solution to extend the life of the handset battery, but this has its own drawbacks such as increased risk of catastrophic battery failure. Furthermore, as the radio frequency (RF) transceiver has the most substantial energy consumption in wireless handsets during the call scenario, compared to the backlight, the liquid-crystal display, or even the CPU [3], wireless handset transceivers' energy consumption has received an increased attention from the wireless research community [4–42].

In the wireless handset transceiver, the energy is consumed mostly in the PA, which transmits data to the receiver, and in the other circuits of the transceiver. It is important to study and model

these elements to reduce the consumed energy. Therefore, in this work, we study the PA energy consumption thoroughly, as well as the other circuits energy.

PAs can be categorized as linear or non-linear. Linear PAs such as class A, class AB, and class B have a considerable operating linear range where they provide the linear amplification required by linear modulations; non-linear PAs such as class E and class F have no linear operating range and are thus more suitable for constant envelope modulations [20]. Linear PAs have lower maximum efficiency than non-linear PAs; however, because linear modulations can provide higher spectral efficiency, such as multilevel quadrature amplitude modulation (MQAM), linear PAs will be considered herein.

Class A PAs are the most common type of linear PA due to mainly the simple design, the low signal distortion levels, and due to having the highest linearity range over the other amplifier classes. However, staying in the "on" situation all the time, even without an input signal, creates tremendous amount of wasted (heat) energy, which leads to an efficiency as low as 0.35.

Class B PAs provide a solution for the low efficiency and the heating problem associated with class A PAs, where the efficiency of class B PAs is around 0.7; however, the price paid for this improvement is in a smaller linear operating region.

Class AB PAs are, as the name suggests, a combination of class A and class B PAs in term of efficiency and linearity, with efficiency reaching about 0.5 to 0.6. Therefore, the AB PA class is currently one of the most commonly used types in wireless handsets.

Modulation signals need to stay in the linear range of PAs to avoid crossing over to the non-linear region and face serious in-band distortion. On the other hand, to obtain the highest PA efficiency, for all the three PA classes mentioned above, a signal needs to be amplified near the top level of the linear range, just before the non-linear region. As multiple amplitudes technique,

MQAM usually generates peaks that may cross the linear margin. Such a signal requires reducing the signal power level to keep the peaks out of the non-linear region, which is called *power back-off*. Therefore, the peak to average power ratio (PAR) may result in reducing the already-low efficiency and increasing the amount of energy consumption in the PA as heat [43]. On top of that, the efficiency of class A PA decays faster than that of class B when reducing the power output level, cf [43, 44]. Hence, PAs must be adequately modeled to locate the minimum energy consumption for wireless handsets.

On the other hand, the multiple antenna systems that are currently used to increase the spectrum efficiency [26–29, 45, 46], can also be use to decrease the energy consumption in the wireless handset device. Multiple-input-multiple-output (MIMO) techniques are used to increase the bit rate of the system and offer high quality links when compared to traditional single-input-single-output (SISO) systems. There are two MIMO schemes: spatial diversity schemes to increase the reliability of the transmission link and spatial multiplexing (SM) schemes to increase the data rate. Spatial diversity schemes, which can be at the transmitter and/or at the receiver, are employed to mitigate fading. By sending multiple copies of the same data across independent fading channels, the impact of fading on each copy will be different. This process guarantees that at least one of these copies will experience less fading compared to the rest, which increases the probability of receiving the data correctly. In SM, each spatial channel can carry independent pieces of data leading to an increase the data rate of the system. If the scattering by the environment is rich enough, several independent sub-channels are used in the same allocated bandwidth. Therefore, the multiplexing gain comes at no additional cost on bandwidth or power. However, by using spatial multiplexing, the benefits of diversity will diminish as all antennas are used for spatial multiplexing. The tradeoff of SM–spatial diversity on the capacity of the system has been discussed

in [45]. However, the impact of such a tradoff on the wireless handset spectral and energy efficiency just starting to getting the attention it deserves.

1.1 Contributions and Outline of the Following Chapters

In the energy efficiency literature, two research teams provided a thorough analysis of wireless handset transceivers: Cui et al. in [6, 7], and Li et al. in [8, 9]. The models of Cui focused mostly on wireless sensor networks at short distances, where throughput is not a significant issue as in wireless cellular systems. Furthermore, the channel that was considered in the model is a basic additive white Gaussian noise (AWGN) (no small scale fading was considered); and the impact of PAR on the PA via modulation pulse had been neglected. The effects of PAR on the wireless handset transceiver and some of the RF components such as digital-to-analog converter (DAC), analog-to-digital converter (ADC), are studied in Li models in [8, 9]; however, this investigation considered only a short distance of 10 m between the transmitter and receiver. Furthermore, the impact of modulation order on energy efficiency is neglected or is not clear enough. The modulation order is crucial as it is the number of bits per symbol and it is an essential indicator for spectral efficiency. Another limitation of the recent works is considering only class A PA in the transceiver, which is simplistic and outdated.

The objective of this work is to develop an advanced energy consumption model for wireless cellular systems in Rayleigh fading channel that takes into account a broad range of parameters. As such, we aim to fill important gaps in the previous studies mentioned above. Central to this task is the importance of an accurate PA model, due to the PA's dominance in transceiver energy consumption. We strive for this accuracy in two ways:

1. We treat the impact of transmitted energy and dissipated energy (heat) separately, so the effect of each is clearly understood. To clarify, the energy model of the PA itself is not new, but arranging the PA energy into two separate terms allows us to be more exact in isolating the energy impact of specific parameters, such as modulation order, modulation pulse shape, and transmission distance.

2. We model efficiency of multiple linear PA classes depending on their characteristics, such as associated maximum drain efficiency and decay rate, as a function of modulated order, and transmission distance—which to the best of our knowledge is a first for wireless handset models to jointly study these parameters—in order to provide practical design insights.

In Chapter 2, based on the above motivations, our energy consumption model takes into account parameters, such as transmitted energy, dissipated energy, other circuit energies, constellation size, modulation pulse roll-off factor α, normalized transmission time (or transmission duty cycle), Rayleigh fading channel, PA's maximum drain efficiency $\eta_{\max}$, PA's efficiency decay rate λ, and transmission distance d. We use our model to generate a comprehensive set of numerical results that give design insights such as: Which modulation order/normalized transmission time pairing is the most energy efficient for a given transmission distance? How much power back-off is required for the PA to transmit a high modulation order? What is the impact of PA selection on energy consumption as a function of modulation order and normalized transmission time? Chapter 2 contributes significant practical enhancements, which include the Rayleigh fading, the modeling of PA efficiency with the appropriate drain efficiency and decay rate, factoring the PAR into its components, and determining the optimum modulation order for energy efficiency at a given distance. These enhancements allow our model to answer questions left by previous studies.

Another key issue that is considered in Chapter 2 is to model the separate components of PAR. Such modeling has often been limited to the signal constellation alone, as in [6, 10]. A neglected-yet-significant component of PAR stems from the modulation pulse, which has a roll-off factor and is typically factored into separate square-root-Nyquist pulses–also called square-root-raised cosine pulses (SRRC)–at the transmitter and the receiver, (the model of Li in [8, 9] ignores this factorization). Accurate consideration of the roll-off factor is essential for correct modeling of energy consumption, where the roll-off factor α impacts transmit energy via the required bandwidth, and the PA dissipated energy via PAR of SRRC: $\mathrm{PAR}_{\mathrm{SRRC}}(\alpha)$. Through this separation, we also able to model some of the other circuits in the handset, specifically DAC, and ADC as a function of modulation order.

In Chapter 3, we discuss *power control*, which can, similar to PAR, cause power back-off in PAs. Power control[1] is a technical mechanism that is used to achieve better wireless system performance by preventing the unwanted interference that happens due to the near-far problem at the receiver [14]. The idea of this mechanism is to transmit low power level from handsets that are close to the base station and increase that power level gradually while the handset moves away, to ensure an equal power level at the base station receiver. In Chapter 3, we model the impact of power control on energy consumption in which we determine the influence of d on PA efficiency, which is similar to the impact of b via PAR, as discussed in Chapter 2. Moreover, as PAR represents the impact of the *system level* and power control represents the impact of the *network level* on PAs energy consumption, studying these two aspects together can help us to better understand the energy consumption of PAs and create new approaches that mitigate/utilize the impact of power

[1] In our work, we deal with power control that associated with large scale fading, the small scale fading can be addressed via the water filling scene as in [47].

control.

In Chapter 4, we develop our model to cover the impact of MIMO technique on the energy consumption; this time, we move from reducing the PA dissipated energy to reducing the transmit energy itself, which will eventually reduce the dissipated energy. The impact of the two MIMO schemes (spatial diversity and SM) on the transmit energy is measured in energy per bit in two cases: i) with channel state information, and ii) without channel state information, as the performance of each scheme may vary with the CSI. After that, we extend the MIMO model to observe the benefits of having massive MIMO antennas at the base station on the transmit energy of wireless handsets comparing to that of a conventional MIMO case. Cui in [46], also investigates the impact of MIMO on the energy consumption of wireless handsets with a fading channel consideration. However, the investigation covered only the MIMO diversity, without considering SM or a massive MIMO.

Figure 1.1 summarizes the contributions of this dissertation via exhibiting the limitations of the previous works, presenting the new outcomes compared to the literature, and outlines all the chapters accordingly.

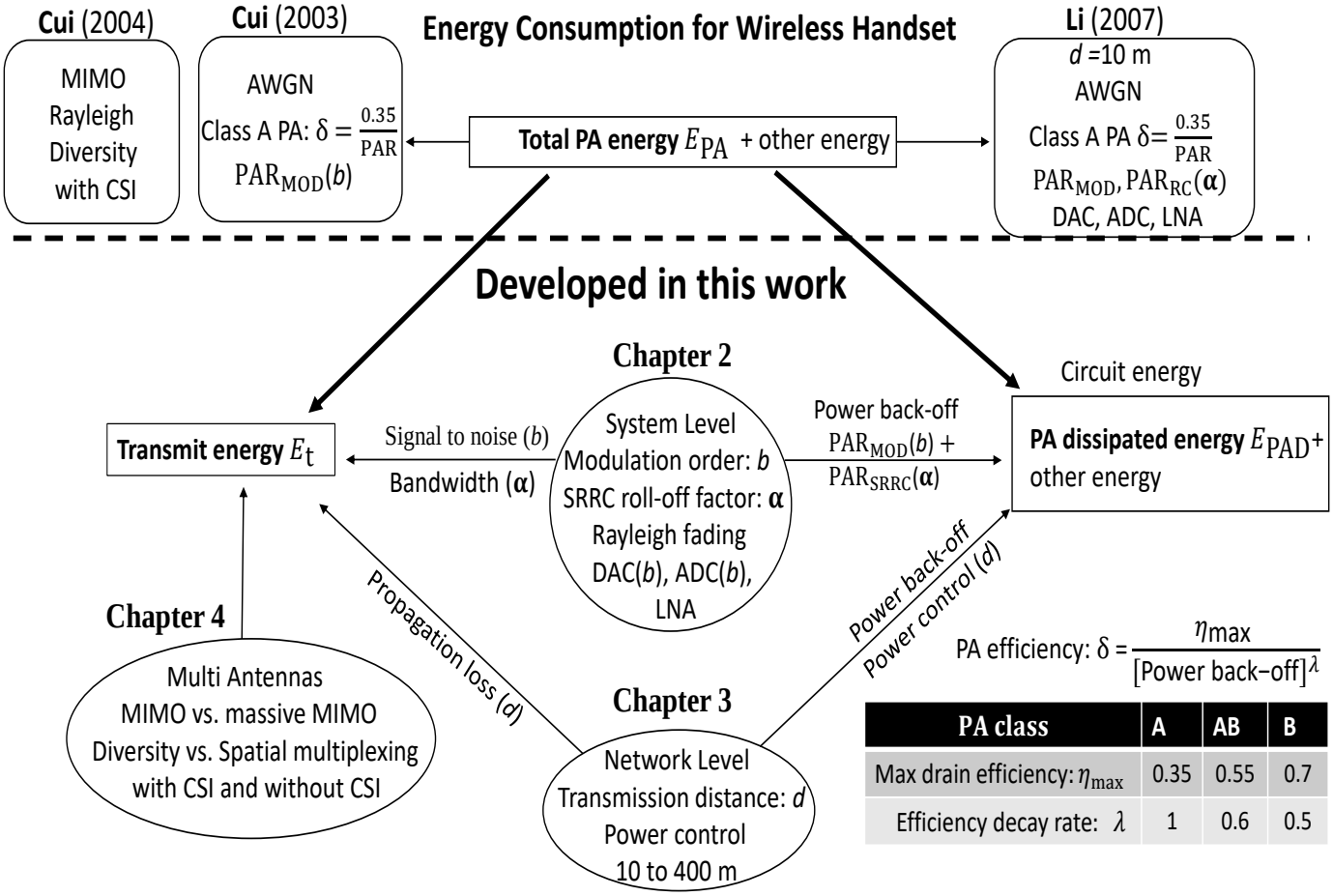

Figure 1.1: Contributions Visualization with Chapters outline. Where the total PA energy consumption E_{PA} = transmit energy E_{t} + PA dissipated energy E_{PAD}. Modulation order: b is the number of bit per symbol in MQAM signal. $\mathrm{PAR}_{\mathrm{MOD}}$ is the peak to average ratio (PAR) of modulation. $\mathrm{PAR}_{\mathrm{SRRC}}(\alpha)$ is the PAR of square root raised cosine (SRRC) pulse shape with a roll-off factor of α, while $\mathrm{PAR}_{\mathrm{RC}}$ is PAR of raised cosine (RC). DAC, ADC, and LAN are the digital-to-analog converter, analog-to-digital converter, low-noise-amplifier, respectively. AWGN is the additive white Gaussian noise channel. δ is the PA efficiency. CSI is the channel state information.

Chapter 2

Energy Modeling and Evaluation

2.1 Key Points of the Chapter

- Provide a detailed model for time and energy (for power amplifier (PA) and other circuits) in case of active and sleep wireless handsets.

- Discuss the PA transmit energy and PA dissipated energy as heat separately. In which we derive the transmit energy as a function of modulation order, modulation pulse shape, and transmission distance. We also model the PA dissipated energy as a function of modulation order and modulation pulse shape for different linear PAs.

- Model the efficiency for various linear PAs based on maximum drain efficiency and the decay rate, through which the impact of both: 1) peak-to-average-power ratio (PAR) of multilevel quadrature amplitude modulation (MQAM) signals and 2) PAR of square root raised cosine pulse shape on PA dissipated energy are stated and analyzed.

- In the other circuits energy, we also discuss the energy of digital to analog converter (DAC)

and analog to digital converter (ADC) as a function of modulation order.

- Derive the total energy efficiency formula as a function of modulation order for various transmission distances.

2.2 System Model

In this chapter, we consider a transmission range of $d = 10$ to $d = 200$ m to cover short and long distance communications, respectively. We select the target probability of error in the intended receiver as $\bar{p}_{e_b} = 10^{-3}$. We consider the Rayleigh fading channel, as a small scale fading, as well as the large scale fading. We consider MQAM signal constellations of size M and constellation order $b = \log_2\{M\}$. We do not consider error control coding and we assume perfect timing and carrier synchronization.

In this section, we outline the RF transceiver blocks of our model, the operation modes, and the corresponding energy consumption model.

2.2.1 Transceiver Blocks

The RF transceiver's circuit structure typically includes many RF components as shown in Figure 2.1, such as the PA, digital-to-analog converter (DAC), analog-to-digital converter (ADC), low-noise-amplifier (LNA), local-oscillator (LO), filters, mixers, etc. These components can be active or inactive depending on the operation mode of the handset.

2.2.2 RF Transceiver Operation Modes

The transceiver operates in one of two modes:

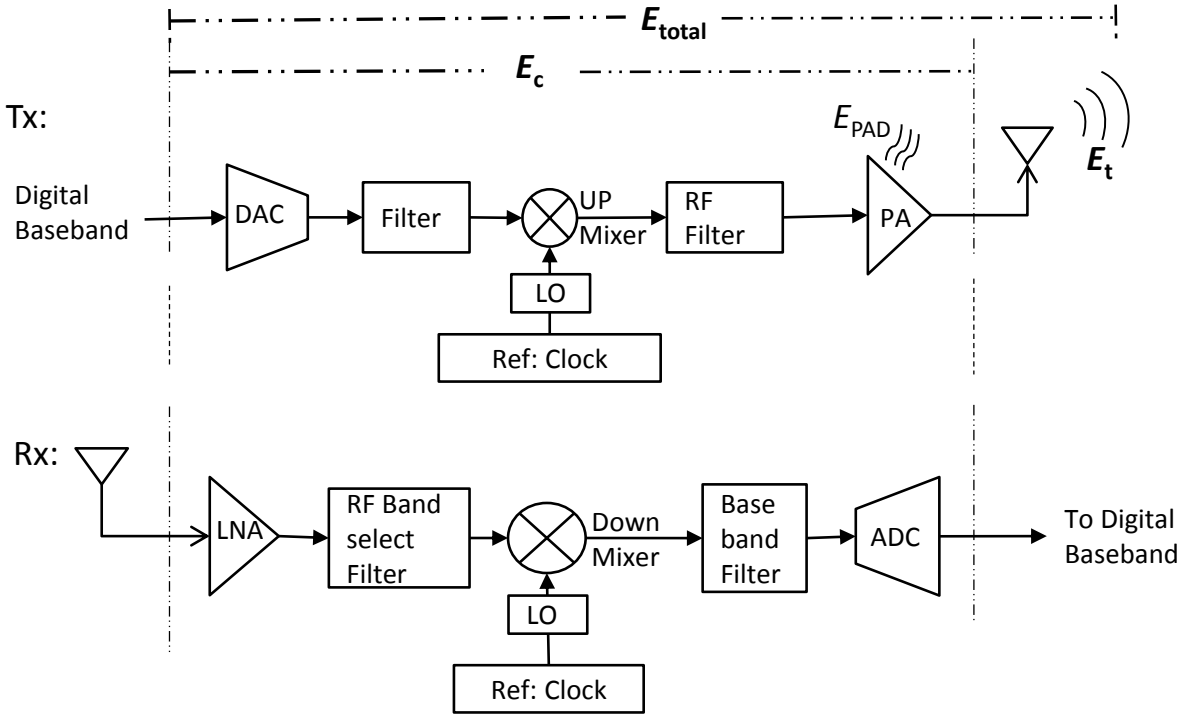

Figure 2.1: Block diagram of the transceiver circuit.

Table 2.1: System parameters.

Components	Symbol	Assumed value
Modulation order– under study	b	$\in \mathbb{N}$
Roll-off factor–under study	α	$0-1$
Overall cycle duration	T	100 mSec
Total bits to be transmitted	L	14 Kbit
Symbol rate	R_{s}	100 KHz
Average bit error rate	$\bar{p}_{e_b}$	10^{-3}
Thermal noise	$\sigma^2 = N_o/2$	-147 dBm/Hz
Receiver noise figure	N_{F}	10 dB
Propagation loss factor	k	2.6
Other fixed power	P_{fixed}	288 mW
Handset sleep mode power	P_{sleep}	50 mW
Link margin	M_l	4dB

1. *On* (active) mode: when all circuits are active and the signal is being transmitted, with a time of T_{on}, a power level of P_{on}, and energy consumed of $E_{\text{on}} = P_{\text{on}} T_{\text{on}}$.

2. *Sleep* (inactive) mode: when there is no signal to be transmitted and all circuits are off, with a time of T_{sleep}, a power level of P_{sleep}, and energy consumed of $E_{\text{sleep}} = P_{\text{sleep}} T_{\text{sleep}}$.

Accordingly, the total energy consumption of the transceiver is the sum of the energies of these two modes:

$$E_{\text{total}} = E_{\text{on}} + E_{\text{sleep}} = P_{\text{on}} T_{\text{on}} + P_{\text{sleep}} T_{\text{sleep}}, \tag{2.1}$$

where P_{sleep} is listed in Table 2.1 and E_{on} is developed further in this section. The overall cycle duration is $T = T_{\text{on}} + T_{\text{sleep}}$. We define the normalized *on* time as $\varepsilon = T_{\text{on}}/T$. The value of ε determines the relative time (or duty cycle) required for the circuits to send a fixed number of L information bits. One extreme case is to have $T_{\text{on}} \to T$, i.e., $\varepsilon \to 1$; this is where the circuits never go to sleep. Here the lowest modulation order is selected because the transmitter has sufficient time to transmit the L bits. The other extreme case is to have $T_{\text{on}} \to 0$, i.e., $\varepsilon \to 0$ and $T_{\text{sleep}} \to T$; this is where the modulation order must approach infinity ($b \to \infty$) in order to transmit the L bits. For the sake of practicality, we constrain the transceiver to be in the *on* mode at least 10% of the time, i.e., $\varepsilon \in [0.1, 1]$, because an arbitrarily large modulation order is infeasible.

There are subtle tradeoffs between the transmission duty cycle, modulation order, and overall energy consumption. As such, it is important to establish the relationships between the many parameters in the energy consumption model. The minimum value of T_{on} is a function of b, L, and the symbol rate R_{s}, and is

$$T_{\text{on}} \geq \frac{L}{R_{\text{s}} b}. \tag{2.2}$$

The inequality stems from the fact that b must assume integer values. Solved for b, this expression becomes

$$b = \left\lceil \frac{L}{R_{\mathrm{s}} T_{\mathrm{on}}} \right\rceil = \left\lceil \frac{L}{R_{\mathrm{s}} T \varepsilon} \right\rceil, \tag{2.3}$$

where $\lceil y \rceil$ denotes the smallest integer greater than or equal to y (commonly referred to as the ceiling operator). R_{s} is related to the bandwidth of the system, B, via the dimensionality theorem for MQAM [20], where for a raised cosine pulse with roll-off factor α, the bandwidth is given by

$$B = (1+\alpha) R_{\mathrm{s}}. \tag{2.4}$$

The impact of α on the PAR and energy consumption will be discussed in Section 2.4.3. The values of T, R_{s}, and L are fixed and are listed in Table 2.1.

2.2.3 Modeling the Energy Consumption

In the *on* mode,[1] the energy consumption in the literature [6–10] is usually divided into two main parts: (a) the total PA energy consumption, E_{PA}, which includes the transmit energy E_{t} and the impact of PA efficiency δ as:

$$E_{\mathrm{PA}} = E_{\mathrm{t}} / \delta; \tag{2.5}$$

and (b) the energy consumption of all other transceiver block circuits, which are mentioned in Section 2.2.1 excluding the PA, and form E_{others}. In our model, as shown in Figure 2.1, we rearrange this combination as (a) the transmit energy E_{t}, and (b) the total circuit energy E_c, which includes E_{others} *and* the impact of PA efficiency δ in the form of waste heat dissipated by the PA, E_{PAD}. The

[1] E_{sleep} is no longer investigated, but it is considered in all the total energy results of this work.

steps going from previous models to ours are

$$\begin{aligned} E_{\text{on}} = & \quad E_{\text{PA}} + E_{\text{others}} \\ = & \quad E_{\text{t}}/\delta + E_{\text{others}} \\ = & \quad (E_{\text{t}} + E_{\text{PAD}}) + E_{\text{others}} \\ = & \quad E_{\text{t}} + (E_{\text{PAD}} + E_{\text{others}}) \\ = & \quad E_{\text{t}} + E_{\text{c}}. \end{aligned} \tag{2.6}$$

It is worth noting that separating PA efficiency, δ, from E_{t} and isolating it entirely in E_{PAD} is a key step in developing our model. Because of this step, it is easier to identify the true impact of parameters such as b and d on the different energy terms inside the transceiver. For example, the modulation order b affects E_{t} via the required probability of bit error p_{e_b}, while it affects E_{PAD} via the amount of PAR. Furthermore, the impact on the dissipated energy due to parameters such as maximum drain efficiency and decay rate for different classes of PAs will be easier to define.

The following three sections of this chapter will discuss the energy terms E_{t}, E_{PAD}, and E_{others}, respectively. Generally, the transmitted energy, $E_{\text{t}} = P_{\text{t}} T_{\text{on}}$, depends on many factors such as transmission distance d, propagation loss factor, system bandwidth B, receiver noise figure N_{F}, required p_{e_b} at the receiver, modulation order b, and T_{on}. The value of E_{PAD} still depends on E_{t} with respect to δ as

$$E_{\text{PAD}} = E_{\text{PA}} - E_{\text{t}} = (1/\delta - 1)\, E_{\text{t}}. \tag{2.7}$$

For example, if $\delta = 0.25$, the amount of $E_{\text{PAD}} = 3E_{\text{t}}$. E_{others} that is shown in Figure 2.1 is nearly fixed for a given communication distance, d; however, there is some variation because the DAC and ADC energy consumption varies with modulation order b [48]. As such, we enhance our

model by treating these separately, which yields

$$E_{\text{others}} = (P_{\text{DAC}} + P_{\text{ADC}} + P_{\text{fixed}})\, T_{\text{on}}, \tag{2.8}$$

where the value for P_{fixed} is listed in Table 2.1.

It is important to mention that we deal with the uplink scenario; therefore, as we determine E_{t}, the transmitter is in the handset and the receiver is in the base station. However, as we deal with E_{c}, we calculate the energy consumed in both the transmitter and receiver sides of the handset, in order to determine the total energy consumption per bit.

2.3 Transmitted Energy E_t

To achieve a specific constraint on the average probability of bit error at the base station receiver, say $\bar{p}_{eb} = 10^{-3}$, it is necessary to determine the transmit energy, E_{t} required for the handset PA for transmission over Rayleigh fading channel. The exact analytical formula for the probability of error for MQAM in the Rayleigh fading channel is provided in the literature [49, 50]. However, because of the complexity in determining E_{t} as a function of $\bar{p}_{eb}$, we do not consider using the exact formula of [49] herein. In this chapter, we derive a simple general formula for MQAM (for even and odd b) based on the derivation that is provided in [45, Section 3.1], and [51, Eq. 6.58] for $b = 1$ and $b = 2$, which are binary phase shift keying (BPSK) and quadratic phase shift keying (QPSK), respectively. The derivation is accomplished by taking the average of the probability of error over the Rayleigh fading probability density function.

For coherent detection, the average probability of error for MQAM in the presence of Rayleigh

fading is

$$\bar{p}_{eb} = \mathbb{E}_h \left\{ W \cdot \mathrm{Q}\left(\sqrt{Z \cdot |h|^2 \mathrm{SNR}} \right) \right\}, \tag{2.9}$$

where SNR is the signal to noise ratio at the receiver and $\mathrm{Q}(\cdot)$ is the Gaussian Q-function. For $b \in \text{even}(\mathbb{N})$ we have $Z = \frac{3}{2^b - 1}$ and $W = \frac{4}{b} \cdot \left(1 - \frac{1}{\sqrt{2^b}}\right)$; and for $b \in \text{odd}(\mathbb{N})$ we have $Z = \frac{6}{2 \cdot 2^b - 1}$ and $W = \frac{4}{b} \cdot \left(1 - \frac{3}{2 \cdot 2^b}\right)$ [52, Eq. 6.45]. $\mathbb{E}_h\{\cdot\}$ is the expected value with respect to the distribution of the channel gain $|h|^2$. As we show in Appendix A, with a unit Rayleigh fading channel gain, the probability of error for MQAM is:

$$\bar{p}_{eb} = W \cdot \left(\frac{1}{2} \cdot \left(1 - \sqrt{\frac{Z \cdot \mathrm{SNR}}{2 + Z \cdot \mathrm{SNR}}} \right) \right). \tag{2.10}$$

To find the required SNR at the receiver, we can write:

$$\mathrm{SNR}(b) = \frac{2}{Z} \cdot \left(\frac{W}{4\, \bar{p}_{eb}} - 1 \right) \approx \frac{W}{2Z} \frac{1}{\bar{p}_{eb}}, \tag{2.11}$$

where the approximation is valid for a very low probability of error, i.e., $\bar{p}_{eb} \leq 10^{-3}$. We see that for a fixed target $\bar{p}_{eb}$, SNR reduces to a function of only b. From the SNR, we can obtain the received power as

$$P_{\mathrm{r}}(b) = 2B\sigma^2 N_{\mathrm{F}}\, \mathrm{SNR}(b), \tag{2.12}$$

where N_{F} is the noise figure of the receiver, $\sigma^2 = \frac{N_0}{2}$ is the noise variance, and N_0 is the noise power spectral density. B is the system bandwidth. At distance d, to achieve $P_{\mathrm{r}}(b)$ at the base station the

transmitted power from our wireless handset must be

$$P_{\mathrm{t}}(b,d) = P_{\mathrm{r}}(b)\ G(d), \tag{2.13}$$

where $G(d)$ is the distance-based path-loss component[2] (i.e., large scale fading)

$$G(d) = d^k G_1 M_l, \tag{2.14}$$

where k is the propagation loss factor; M_l is the link margin compensating for the additive background noise or interference; G_1 is the reference path loss attenuation at $d = 1$ m from the transmitter, and is assumed here to be $G_1 = 66$ dB [14]. In practice, k and G_1 vary greatly with the environment, carrier wavelength, base station and handset heights from the ground, and antenna gains. Equation (2.13) shows the PA transmit power depends on two main parameters b, and d. Thus, E_{t} can be obtained as

$$E_{\mathrm{t}}(b,d) \stackrel{\Delta}{=} P_{\mathrm{t}}(b,d)\ T_{\mathrm{on}} \approx \frac{W}{Z\bar{p}_{eb}} B\sigma^2 N_{\mathrm{F}} G(d) T_{\mathrm{on}}. \tag{2.15}$$

Figure 2.2 captures the relationship between E_{t} and T_{on} and includes the dependence of b on T_{on} [see (2.3)]. The y-axis of the figure represents the energy consumption per bit, in units of dBmJ (decibels relative to a millijoule, $10\log_{10}\{1000\ \mathrm{Energy}/L\}$). The x-axis represents the normalized transmission time $\varepsilon = T_{\mathrm{on}}/T$, which corresponds to how long the device will remain in the **on** mode compared to the sleep mode. Figure 2.2 shows that to send L bits in a short period of time, say $\varepsilon = 0.24$, the required value of b, according to (2.3), is 6 (i.e., 64-QAM) or higher and the

[2]We consider a simple path-loss model for general tradeoff analysis.

required E_t is around 1 dBmJ per bit. However, to send the same L bits in a longer period of time, such as $\varepsilon = 0.8$, a lower modulation order can be used, such as $b = 2$ (i.e., QPSK). This in turn reduces the required E_t to around -5 dBmJ per bit, which is much less than that required for $b = 6$. Therefore, increasing ε allows the transceiver to use smaller b and hence consume less E_t. Because b is required to be an integer, as explained in (2.3), the E_t graph in Figure 2.2 takes discrete steps up or down with changing b. Figure 2.2 shows reference curves for a few fixed modulations, such as QPSK, 8-QAM, and 16-QAM. Because E_t continues to increase slightly with increasing T_{on} but b changes only in discrete steps, the optimum T_{on}^* for each modulation order b is the point where b steps down, which is where (2.2) is satisfied with equality.

Figure 2.2 shows that energy efficiency can be achieved at the expense of spectrum efficiency, which matches the famous information theoretic data rate–power consumption cost tradeoff that is shown in [53] and [54] for the additive white Gaussian noise (AWGN) channel. However, the model in Figure 2.2, yields a result better suited to the realities of wireless communication systems because it includes the effect of modulation order (even and odd), fading channel, transmission time, and the transmission distance between the handset and the base station.

Although E_t generally decreases as $\varepsilon \to 1$, the transceiver circuits must operate longer, the impact of which is studied in the following sections.

2.4 Power Amplifier Dissipated Energy: $E_{\mathbf{PAD}}$

As (2.7) indicates, the PA dissipated energy is a function of the PA efficiency, δ, which in turn is a function of the amplifier type and the PA back-off due to the amplitude fluctuations of the modulated signal.

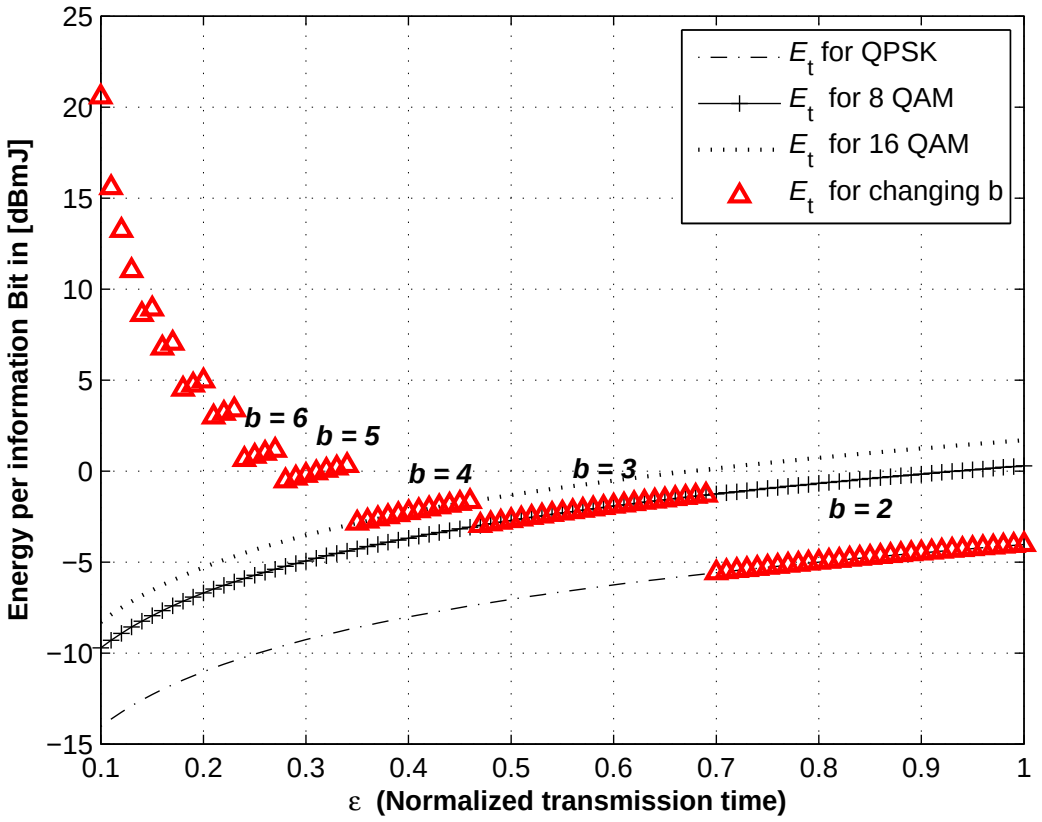

Figure 2.2: Comparison of E_t with different kinds of QAM for Rayleigh fading at $d = 200$ m.

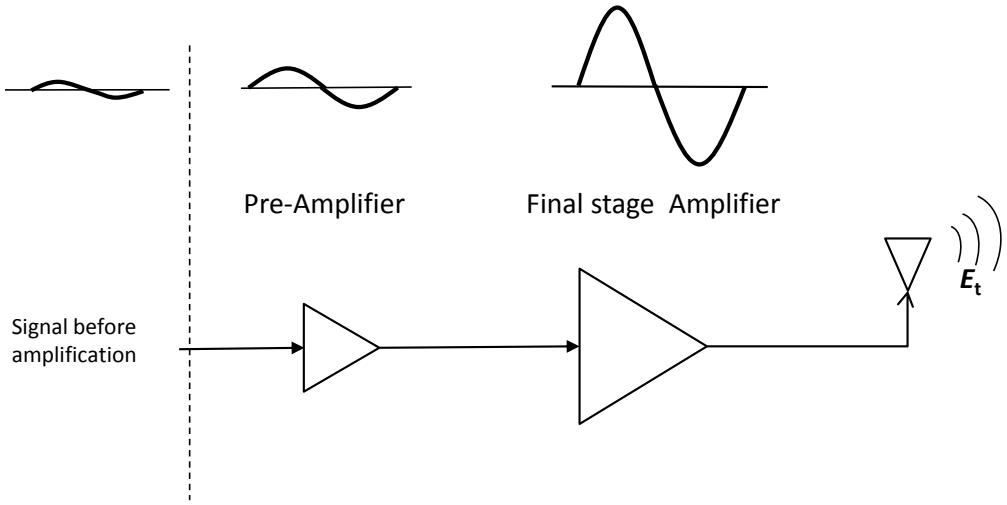

Figure 2.3: Typical wireless communications power amplifier chain.

2.4.1 PA Selection

Figure 2.3 shows a wireless communications amplifier chain consisting of a pre-amplifier followed by a final stage. The role of the pre-amplifier—usually[3] class A—is to drive the input signal power to the proper level required for the final stage. In this dissertation, we use the term "PA" to refer to the final stage because of its dominance in terms of energy consumption and we group the pre-amplifier with the "other" circuits.

PA linearity and efficiency are competing design objectives and both have significant impact on MQAM performance. Because class AB PAs offer an attractive compromise in this design tradeoff, they are a popular choice in wireless handsets. Not only do they provide higher maximum drain efficiency, but class AB PAs also have a lower drain efficiency decay rate as the power is being backed off. A typical maximum drain efficiency for a class A PA is $\eta_{\max} = 0.35$ [43], and for a class AB PA $\eta_{\max}$ is in the range 0.5–0.6 [44, 55]. Drain efficiency is defined as the ratio of

[3]For small signals, the power dissipated by the pre-amplifier is negligible.

the output signal power to the DC power consumed in the PA at a given output power [56]. The PA has the maximum drain efficiency $\eta_{\max}$ when it operates with maximum output power (cf., e.g. [43, Fig. 3.11]). However, it is hard to achieve the maximum drain efficiency with a linear modulation such as MQAM because the envelope of the modulated signal changes with the data. Furthermore, the impact of such modulation on different types of PAs is different, as we see next.

2.4.2 Power Back-off

The characteristic curve of PAs is shown in Figure 2.4, which is based on the Rapp model in [57]. Figure 2.4 has regions labeled for linear and non-linear operation. The non-linearis subdivided into a compression region and a saturation region. For MQAM signals with PAR > 1 (PAR $= 1$ only for BPSK and QPSK because all the points in the I–Q constellation have the same distance from the origin), the signal peak may exceed the limit of linear operation and result in non-linear distortion, the most severe consequence of which is spectral distortion, commonly referred to as "spectral regrowth." There are two main approaches to reduce this distortion [12, 43, 58–61]:

1. The first approach is to clip any peak of the signal that exceeds the region of linear operation. This clipping is illustrated in Figure 2.4 with the shaded signal areas. Because the MQAM constellation points are represented by amplitude and phase, the clipping approach may result in a dramatic loss of information and induce in-band signal distortion [43, 62]. Hence, this approach is not considered herein.

2. The second approach is to use the power back-off procedure, where the average pre-amplifier output level is reduced, which in turn reduces the output level of the final stage. By backing off the same amount as the PAR, the signal peaks remain inside the desired linear range, as

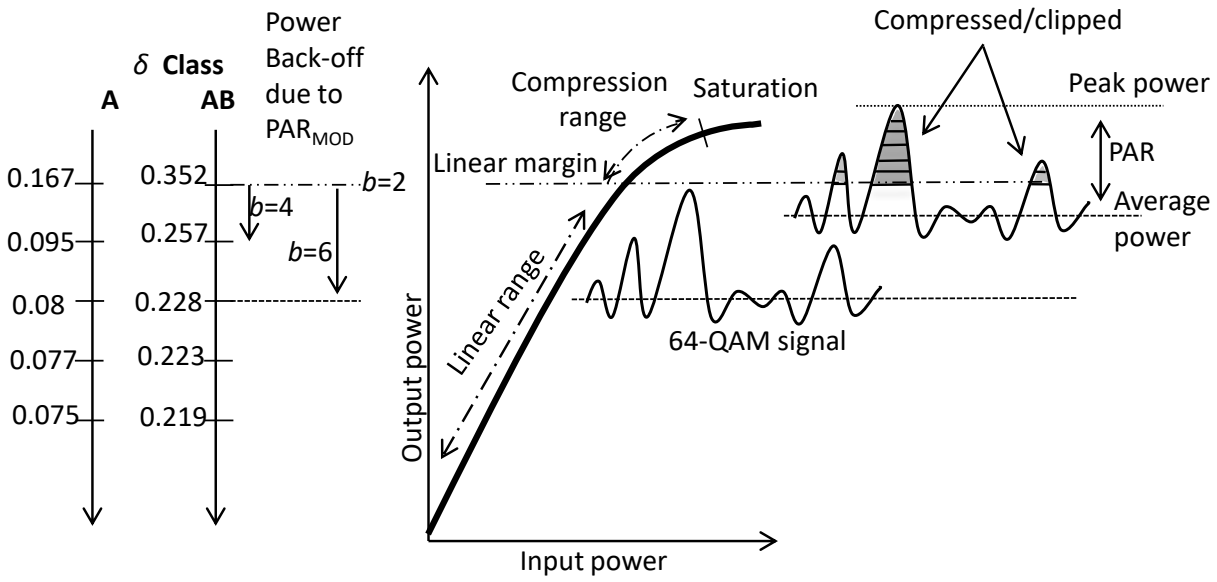

Figure 2.4: Linear PA characteristics, efficiency for class A and class AB PAs, and power back-off for 64-QAM signal.

Table 2.2: Drain efficiency characteristic for different PA classes.

PA type	Efficiency decay rate: λ	Typical drain efficiency [43, 44]: $\eta_{\max}$
Class A	1	0.35
Class AB	0.5–1	0.5–0.6
Class B	0.5	0.7

shown in Figure 2.4. Even though this approach reduces distortion in the modulated signal, the PA efficiency δ decreases proportionally with the PAR/back-off. In this dissertation, we model the impact of power back-off on the efficiency of different types of linear PA—based on the measured patterns for class A and class B PAs that is given in [34, 43]—as

$$\delta = \frac{\eta_{\max}}{(\text{Power back-off})^{\lambda}} = \frac{\eta_{\max}}{\text{PAR}^{\lambda}}, \tag{2.16}$$

where λ is the decay rate, which determines the rate of degradation of the PA efficiency with power back-off. The typical values of $\eta_{\max}$ and λ for class A, B, and AB PAs are listed in Table 2.2. Because the value of λ for the class AB case is in between that of class A and class B, a value of 0.6 is considered in this dissertation. Equation (2.16) can be stated more clearly for class A PAs as

$$\delta = \frac{0.35}{\text{Power back-off}}, \tag{2.17}$$

and for class AB PAs as

$$\delta = \frac{0.55}{(\text{Power back-off})^{0.6}} \, . \tag{2.18}$$

On the left side of Figure 2.4, a numerical scale for (2.17) and (2.18) can be seen, which shows a higher maximum drain efficiency and a lower decay rate for class AB PAs compared to class A PAs.[4]

Other techniques, such as pre-distortion, envelope tracking, Doherty PA [43], etc., are utilized for increasing PA linearity or boosting efficiency, as discussed in the literature [34, 61, 63–66]. However, the processing requirements of these techniques are greater than what current handsets

[4] A complexity study for class A, B, and AB PAs is beyond the scope of this dissertation.

can afford and they are mainly used in base stations; therefore, we leave them for future research.

2.4.3 PAR

Generally, there are different sources of PAR.[5] In QAM modulation, two types of PAR can be found: PAR of the modulation (PAR_{Mod}), which is a function of b, and PAR of the square root raised cosine (SRRC) pulse (PAR_{SRRC}), which is a function α. Therefore, δ can be expressed as a function of b and α as follows:

$$\delta(b,\alpha) = \frac{\eta_{\max}}{\Big(\text{PAR}_{\text{Mod}}(b)\cdot\text{PAR}_{\text{SRRC}}(\alpha)\Big)^{\lambda}}. \tag{2.19}$$

2.4.3.1 PAR of Modulation

PAR_{Mod} is defined as

$$\text{PAR}_{\text{Mod}}(b) = \frac{\max_i(|x_i(b)|^2)}{\text{average}_i(|x_i(b)|^2)}, \quad b \in \mathbb{N}, \tag{2.20}$$

where x_i is a point in the QAM signal constellation. For even b, this can be expressed as a function of b in closed form as:

$$\text{PAR}_{\text{Mod}}(b) = \frac{3\cdot(\sqrt{2^b}-1)}{\sqrt{2^b}+1}, \quad b \in \text{even}(\mathbb{N}). \tag{2.21}$$

The values of $\text{PAR}_{\text{Mod}}(b)$ for $b = 1$ to 16 are listed in Figure 2.5. $\text{PAR}_{\text{Mod}}(b)$ for $b = 1$ (i.e., BPSK) and $b = 2$ (i.e., QPSK) is equal to 1 as all point on the constellation are on the same distance from

[5] Due to its high PAR, orthogonal frequency division multiplexing (OFDM) is usually not used in a handset/uplink scenario, that is why we do not consider that in Chapter 2; however, in Chapter 3, we able to use OFDM as an approach to reduce the impact of power control on the energy.

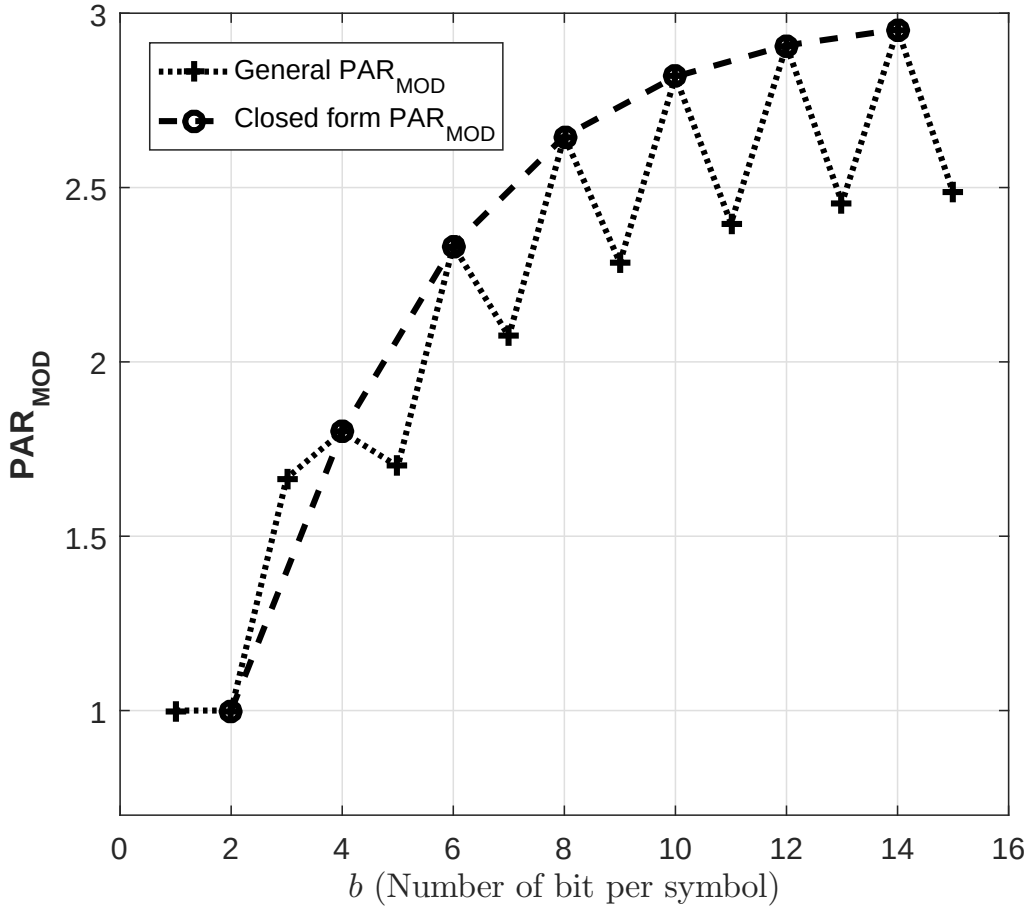

Figure 2.5: PAR_{Mod} as a function of b using the general expression in (2.20) and the closed-form expression in (2.21).

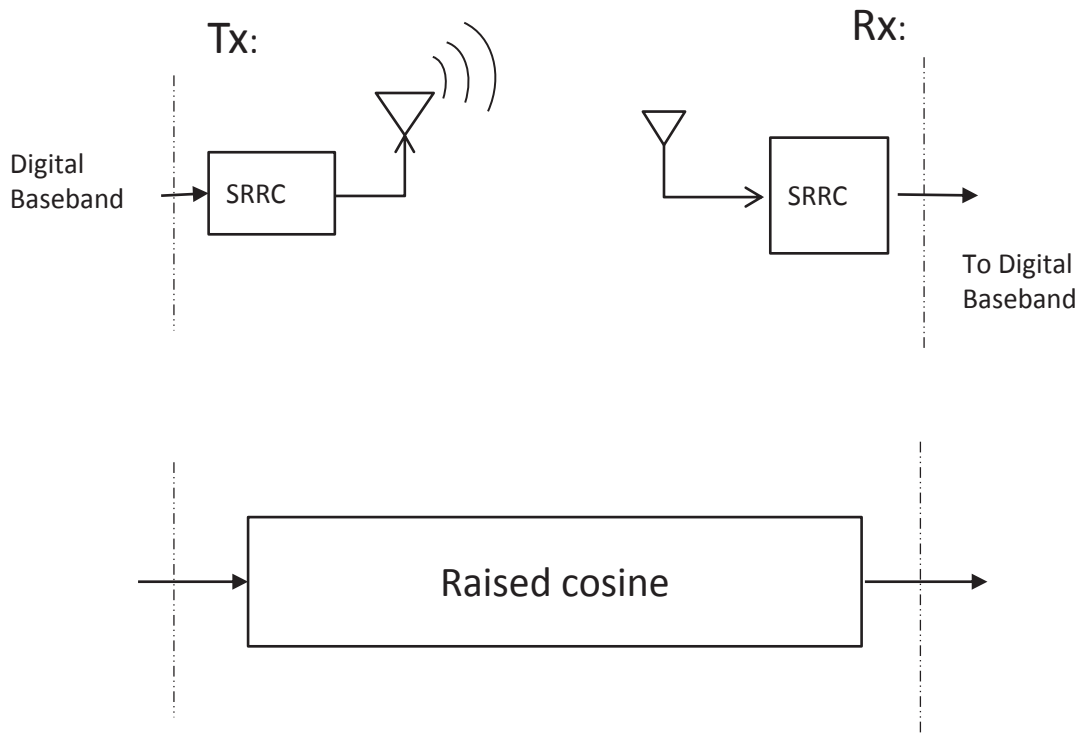

Figure 2.6: The splitting of the raised cosine pulse between the transmitter and receiver using the SRRC pulse.

the origin. $\mathrm{PAR}_{\mathrm{Mod}}(b)$ increases with b and converges to a value of 3 for large modulation orders ($b \geq 10$). This convergence is good news for PA–that have short linearity range, such as class AB and class B–because the PAR/back-off does not grow arbitrarily large with modulation order.

2.4.3.2 PAR due to Roll-off Factor

The raised cosine filter is widely used in communication systems to satisfy the Nyquist no-ISI (inter-symbol interference) criterion [20]. Its use introduces a tradeoff between PAR and bandwidth, the latter being parameterized by the roll-off factor as in (2.4). This tradeoff can be described as follows: for $\alpha = 0$ the system has a higher PAR with a minimum bandwidth of $B = R_s$, while for $\alpha = 1$ the system has a lower PAR with a bandwidth of twice the minimum, $B = 2R_s$.

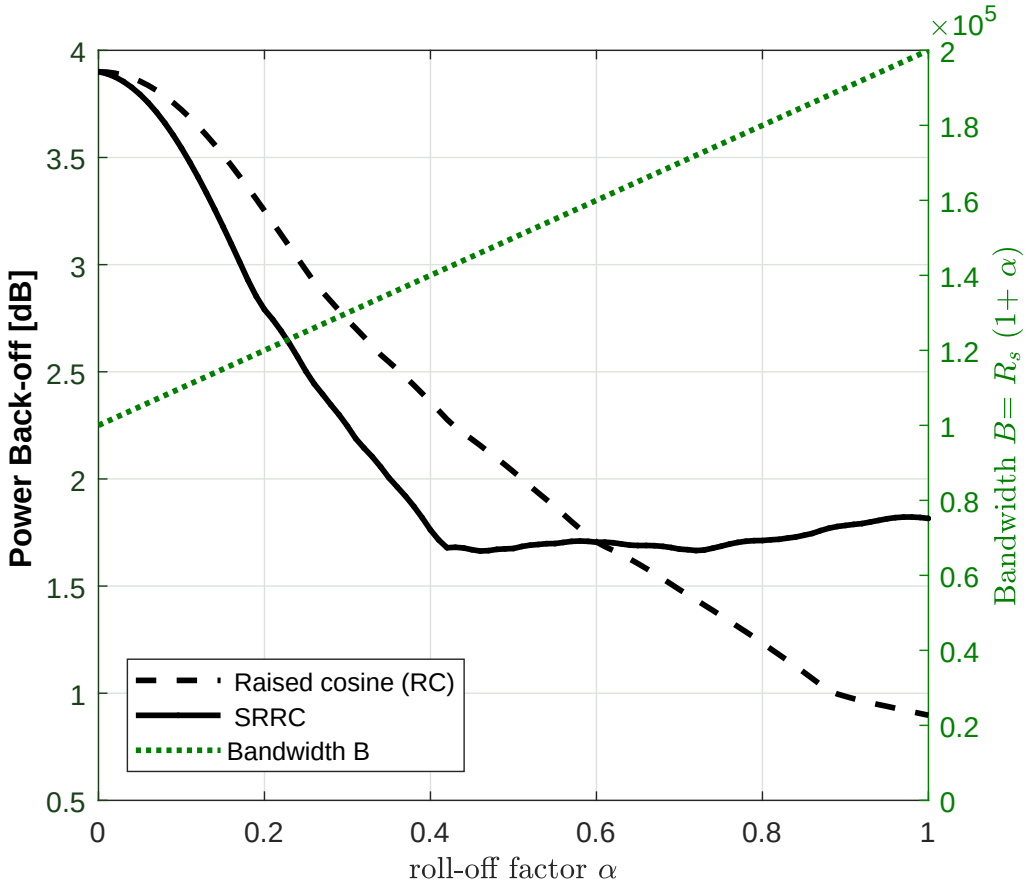

Figure 2.7: Left axis: the power back-off in dB vs. α for raised cosine and SRRC with QPSK ($\text{PAR}_{\text{Mod}} = 1$). Right axis: Bandwidth vs. α.

Many energy efficiency studies, e.g. [8,67], have considered the case of $\alpha = 1$ as a good design choice with respect to PAR. However, this is simplistic as it assumes the raised cosine pulse is located in the transmitter only, when in reality, as illustrated in Fig 2.6, the raised cosine response is often split evenly between the transmitter and receiver; the result of this split response is the SRRC filter [20]. We consider the SRRC herein because of its practicality.

Figure 2.7 shows the power back-off in dB vs. roll-off factor α for the raised cosine (RC) and square-root raised cosine (SRRC) filters, assuming QPSK and a maximum drain efficiency of $\eta_{\text{max}} = 0.55$. The peak and average values used to generate this figure were measured numerically over a signal duration of one million QPSK symbols. The minimum back-off amount—which

Table 2.3: PAR for MQAM [in dB].

b	2	4	6	8	10	12
$\text{PAR}_{\text{Mod}}(b)$	0	2.5	3.7	4.2	4.5	4.5
$\text{PAR}(b, \alpha = 0.42)$	3.5	5.7	6.7	6.9	7	7

corresponds to the minimum PAR_{SRRC}—occurs at $\alpha \approx 0.42$ for SRRC, which differs from the location of the minimum back-off for the raised cosine case ($\alpha = 1$). This value of $\alpha \approx 0.42$ has already been verified to achieve minimum PAR_{SRRC}, both theoretically and numerically, e.g. [60, 68]. However, this is the first instance where this value is identified for optimizing the energy consumption in an energy efficiency model.

The roll-off factor influences E_{PAD} in (2.7) in two different ways: one through the bandwidth and hence E_{t}, and the other through the PA efficiency via (2.16), both of which are captured in Figure 2.7. The left-hand axis shows power back-off and the right-hand axis shows the bandwidth B. The net effect of α on E_{PAD} is plotted in Figure 2.8, which shows that E_{PAD} achieves a minimum value at $\alpha \approx 0.42$. This is true for other signal constellations in addition to QPSK, as shown in Figure 2.8. The amount of energy savings using $\alpha \approx 0.42$ instead of $\alpha = 1$ is around 2 dB, in addition to the bandwidth savings of 29%. Therefore, $\alpha = 0.42$ will be consider for the rest of this dissertation.

□

The overall PAR as a function of modulation order at $\alpha = 0.42$ can be seen in Table 2.3. in the table, we see that with increasing b the value of PAR_{Mod} converges to 4.5 dB (i.e., 3 as seen in Figure 2.5), and the combined PAR, of PAR_{Mod} and $\text{PAR}_{\text{SRRC}}(\alpha = 0.42)$, converges to 7 dB.

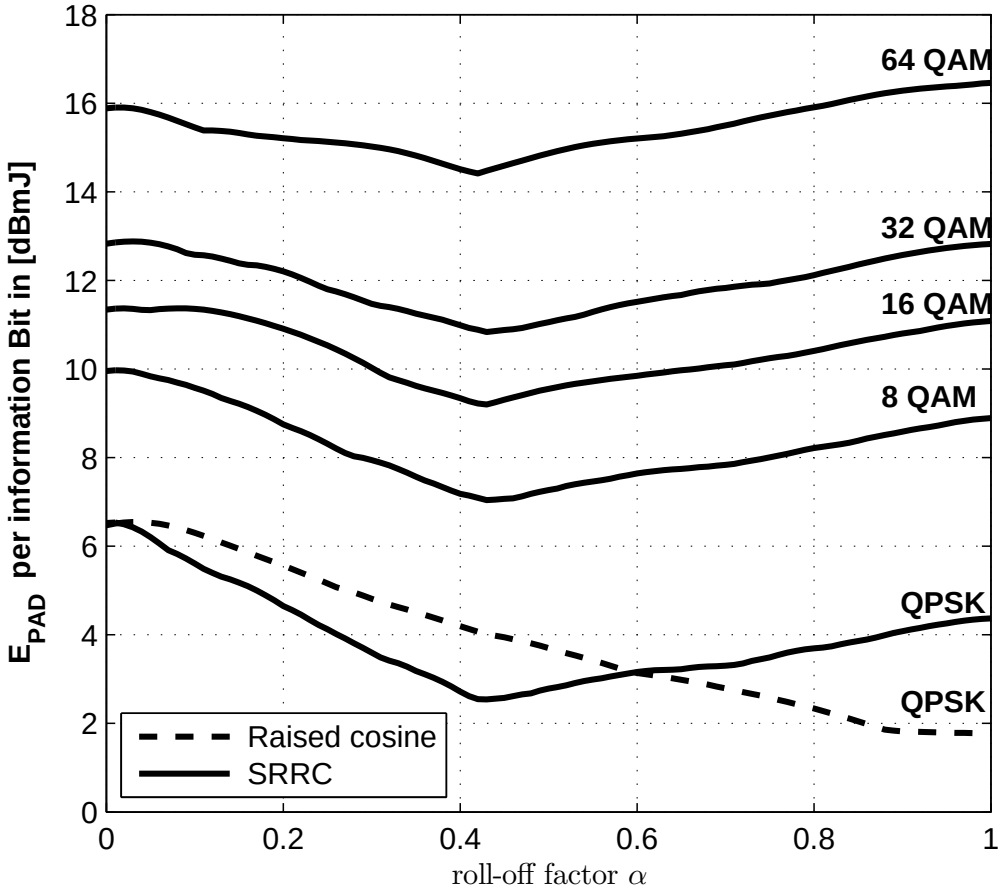

Figure 2.8: E_{PAD} vs. α for different modulation orders.

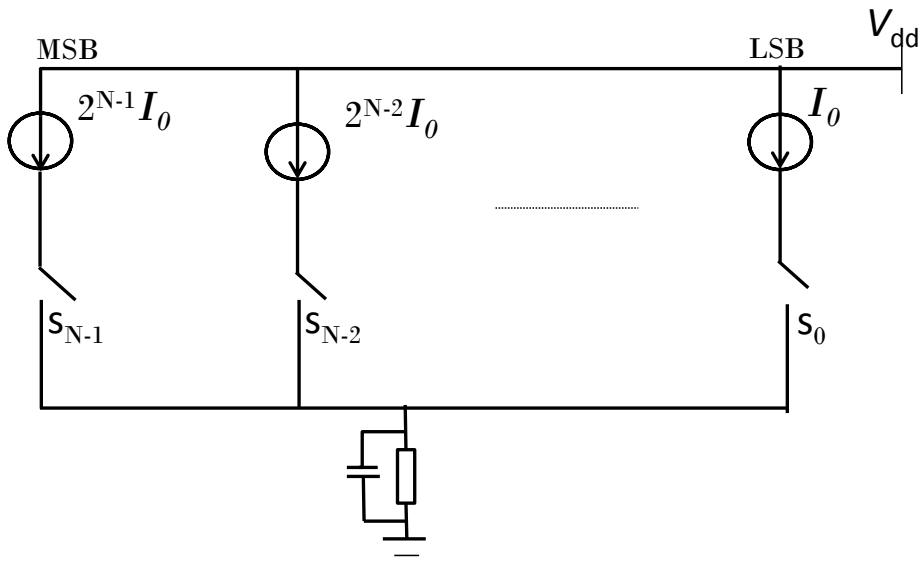

Figure 2.9: Binary weighted current steering DAC.

2.5 Other Circuit Energy: E_{others}

We now develop the terms in (2.8). The reason that we choose to study DAC and ADC, as their energy have a relation to the modulation order via PAR_{Mod} as we see next.

2.5.1 Digital to Analog Converter (DAC)

The DAC is the first block in the signal chain in the transmitter. The current-steering DAC architecture that is shown in Figure 2.9 is considered herein. The power consumption of the DAC has two terms—called static and dynamic [48]—which are

$$P_{\text{DAC}} = \frac{1}{2} V_{\text{dd}} \cdot I_0 \cdot \left(2^{N_{\text{DAC}}} - 1\right) + N_{\text{DAC}} \cdot C_{\text{p}} \cdot B \cdot V_{\text{dd}}^2 \cdot \text{OSR}, \tag{2.22}$$

where V_{dd} is the power supply voltage, I_0 is the unit current source relating to the least significant bit (LSB), OSR is the oversampling ratio, and C_{p} is the parasitic capacitance of each switch [48].

N_{DAC} is the resolution of the DAC in bits. Based on the signal to noise ratio inside the DAC of approximately 42 dB [48], we derive the following expression of N_{DAC} as a function of $\mathrm{PAR}_{\mathrm{Mod}}$

$$N_{\mathrm{DAC}} = \left\lceil 7 + \frac{10\log_{10}\{\mathrm{PAR}_{\mathrm{Mod}}(b)\}}{6.02} \right\rceil. \tag{2.23}$$

Existing models often assume a fixed value of $N_{\mathrm{DAC}} = 8$ or 9 bits, e.g. [6, 8]; however, we allow N_{DAC} to vary in order to more fully capture the energy consumption of the DAC vs. modulation order b. These results can be seen later in Figure 2.11, where the assumed values of the DAC parameters are: $V_{\mathrm{dd}} = 3.3$ V, $I_0 = 10\ \mu$A, $C_{\mathrm{p}} = 1$ pF, and $\mathrm{OSR} = 4$.

2.5.2 Analog to Digital Converter (ADC)

Similar to the DAC, the power consumption of the ADC is expressed as [48]

$$P_{\mathrm{ADC}} = \frac{3V_{\mathrm{dd}}^2 \cdot L_{\min} \cdot B}{10^{-(0.152 \cdot N_{\mathrm{ADC}} + 4.838)}}, \tag{2.24}$$

where $L_{\min} = 0.5\ \mu$m is the minimum channel length of the complementary metal oxide semiconductor (CMOS) technology. For simplicity, we assume N_{ADC} is equal[6] to N_{DAC}.

The term $P_{\mathrm{fixed}}T_{\mathrm{on}}$ in (2.8) models the energy consumption of the remaining circuitry mentioned in Section 2.2.1. The numerical impact of the DAC and ADC on the energy consumption of the wireless handset will be discussed in Section 2.6.2.

[6] In reality, N_{DAC} and N_{ADC} may have different values, because they face different design requirements, such as spectral regrowth, linearity, etc.

2.6 Energy Metrics

2.6.1 Energy Efficiency

The energy efficiency U of the wireless handset, in units of bits per joule, can be expressed as a function of b and d using the model we have developed:

$$U(b,d) = \frac{R(b)}{P_{\mathrm{t}}(b,d) + P_{\mathrm{PAD}}(b,d) + P_{\mathrm{DAC}}(b) + P_{\mathrm{ADC}}(b) + P_{\mathrm{fixed}}}, \tag{2.25}$$

where $R(b) = bR_{\mathrm{s}}$ is the throughput in bits/sec. As discussed earlier, all terms except P_{fixed} change with b and some with both b and d. Equation (2.25) can be written as a function of b for a given d as

$$U(b) = \frac{bR_{\mathrm{s}}}{P_{\mathrm{t}}(b) + P_{\mathrm{PAD}}(b) + P_{\mathrm{DAC}}(b) + P_{\mathrm{ADC}}(b) + P_{\mathrm{fixed}}}. \tag{2.26}$$

Because the second derivative[7] of $U(b)$ with respect to b is $U''(b) < 0$ (see Appendices B and C), $U(b)$ is a concave function with respect to b and has an optimum value (global maximum) at b^* for a given distance d.

Figure 2.10 shows the concavity of $U(b)$ as a function of b for different values of distance d. The figure shows that increasing communication range decreases the energy efficiency for all b and the location of the optimum b^* on the energy efficiency curve converges to $b = 2$. This is because E_{t} and E_{PAD} dominate the total energy consumption at long communication distances.

Mathematically, the optimum energy efficiency over b can be found by solving the following expression:

$$\underset{b}{\text{maximize}} \quad U(b,d). \tag{2.27}$$

[7] $U(b)$ is continuous and differentiable with respect to b; however, it is evaluated only at integer values.

The solution can be determined by taking the partial derivative with respect to b

$$U'(b,d) = \frac{\partial}{\partial b}\Big(\frac{bR_{\mathrm{s}}}{\frac{1}{\delta(b)}P_{\mathrm{t}}(b,d) + P_{\mathrm{DAC}}(b) + P_{\mathrm{ADC}}(b) + P_{\mathrm{fixed}}}\Big) = 0, \tag{2.28}$$

where $\frac{1}{\delta(b)}P_{\mathrm{t}}(b,d) = P_{\mathrm{t}}(b,d) + P_{\mathrm{PAD}}(b,d)$ is the power consumed in the PA. According to Equation (2.15), $P_{\mathrm{t}}(b) \approx \frac{W}{Z\bar{p}_{eb}} B\sigma^2 N_{\mathrm{F}} G(d)$. Hence,

$$\frac{\partial}{\partial b}\Big(\frac{bR_{\mathrm{s}}}{\frac{4}{b}\cdot(1-\frac{1}{\sqrt{2^b}})\frac{2^b-1}{3}\frac{1}{\delta(b)}KG(d) + P_{\mathrm{DAC}}(b) + P_{\mathrm{ADC}}(b) + P_{\mathrm{fixed}}}\Big) = 0, \tag{2.29}$$

where $K = \frac{1}{\bar{p}_{eb}} B\sigma^2 N_{\mathrm{F}}$.

$\delta(b)$ is a function of b via $\mathrm{PAR}_{\mathrm{Mod}}(b)$ by utilizing Eqs. (2.19) and (2.21),

$$\delta(b) = \frac{\eta_{\max}}{\left(\frac{3\cdot(\sqrt{2^b}-1)}{\sqrt{2^b}+1}\mathrm{PAR}_{\mathrm{SRRC}}\right)^{\lambda}}, \tag{2.30}$$

where $\eta_{\max}$ and λ are listed in Table 2.2 for different types of PAs. Now (2.29) can be stated as

$$\frac{\partial}{\partial b}\Big(\frac{bR_{\mathrm{s}}}{(1-\frac{1}{\sqrt{2^b}})\frac{2^b-1}{b}\cdot(\frac{\sqrt{2^b}+1}{\sqrt{2^b}-1})^{\lambda}K_1 G(d) + Q}\Big) = 0, \tag{2.31}$$

where $K_1 = 4/3^{1-\lambda}K\cdot\mathrm{PAR}_{\mathrm{SRRC}}^{\lambda}/\eta_{\max}$, and[8] $Q \approx P_{\mathrm{fixed}}$. The first derivative of the right hand side

[8]This assumption can be justified in order to simplify the optimization formula because the values of $P_{\mathrm{DAC}}(b)$ and $P_{\mathrm{ADC}}(b)$ are small relative to the other power terms in the transceiver.

of Equation (2.31) can be found in Appendix B . The final result is

$$\left(\frac{(2^{b^*}-1)(\frac{\sqrt{2^{b^*}}+1}{\sqrt{2^{b^*}}-1})^{\lambda}}{2\sqrt{2^{b^*}}} + 2^{b^*} \cdot (1 - \frac{1}{\sqrt{2^{b^*}}})(\frac{\sqrt{2^{b^*}}+1}{\sqrt{2^{b^*}}-1})^{\lambda} + \right.$$
$$\left. \left(\sqrt{2^{b^*}} - 2^{b^*} + 2\right) \cdot \frac{\lambda \cdot (2^{b^*}-1)\sqrt{2^{b^*}} \cdot (\sqrt{2^{b^*}}-1)^{2-\lambda} \log\{2\}}{2 \cdot (\sqrt{2^{b^*}}+1)^{3-\lambda}} \right) \tag{2.32}$$
$$= \frac{Q}{G(d)K_1 \log\{2\}}.$$

This equation provides the optimum modulation order b^* for energy efficiency at a given d.

The mathematical solution of (2.32) matches the numerical plot in Figure 2.10. For example, at $d = 10$ the optimum solution is $b^* = 4$, and for large distances, b^* decreases to 2. Equation (2.32) is considered as a modulation order optimization for energy efficiency at different distances and for different PA types.

In Figure 2.10, it is worth noting that the energy efficiency of QPSK ($b = 2$) is slightly higher than that of BPSK ($b = 1$). The explanation of this is that QPSK has double the throughput and double the transmit power, but with the same fixed value of Q. Regarding P_{t}, using the appropriate values of W and Z for each modulation in (2.11), we see that for the same $\bar{p}_{eb}$ the SNR for QPSK is double that of BPSK. And because $\mathrm{PAR}_{\mathrm{Mod}}(1) = \mathrm{PAR}_{\mathrm{Mod}}(2) = 1$, we have $\delta(1) = \delta(2)$; therefore, we can write the energy efficiency of BPSK as

$$U(1) = \frac{R_{\mathrm{s}}}{\delta(1)P_{\mathrm{t}}(1) + Q}, \tag{2.33}$$

which can be written as

$$U(1) = \frac{2R_{\mathrm{s}}}{2\delta(1)P_{\mathrm{t}}(1) + 2Q}. \tag{2.34}$$

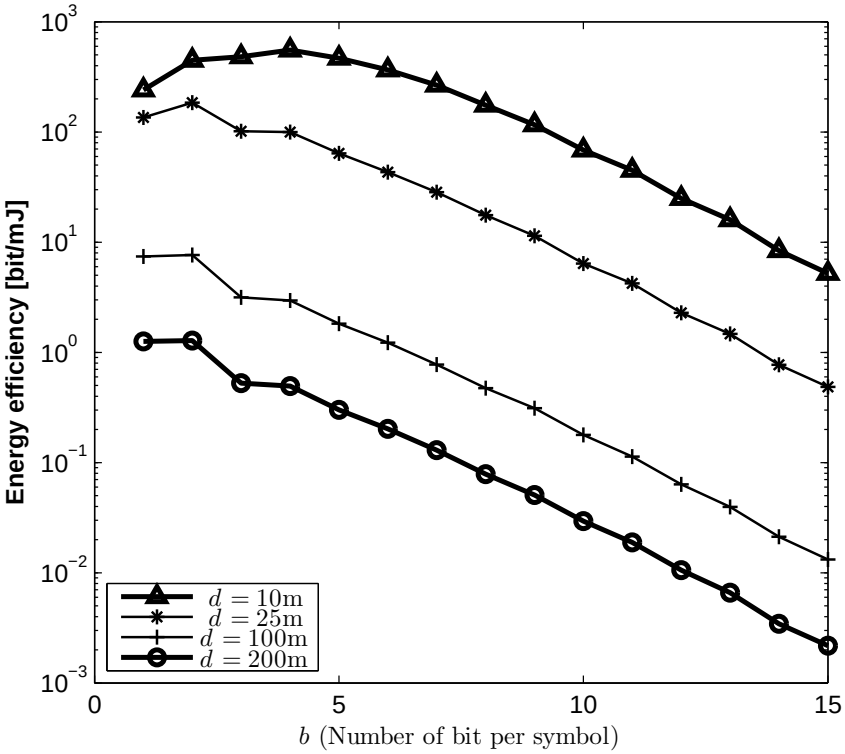

Figure 2.10: Energy efficiency vs. b for various values of distance d.

However, the energy efficiency of QPSK is

$$U(2) = \frac{2R_{\mathrm{s}}}{\delta(2)P_{\mathrm{t}}(2)+Q} = \frac{2R_{\mathrm{s}}}{2\delta(1)P_{\mathrm{t}}(1)+Q}. \tag{2.35}$$

The denominator of (2.34) is greater than the denominator of (2.35) by $Q \approx P_{\mathrm{fixed}}$, and hence the energy efficiency of BPSK is slightly less than that of QPSK.

2.6.2 Energy Consumption

Figures 2.11 and 2.12 show all the energies discussed in our model as a function of normalized transmission time, $\varepsilon = T_{\mathrm{on}}/T$, with the appropriate b [see (2.3)], for short and long distance cases. In both figures, E_{t} and E_{PAD} are generally decreasing with increasing ε because the required b is

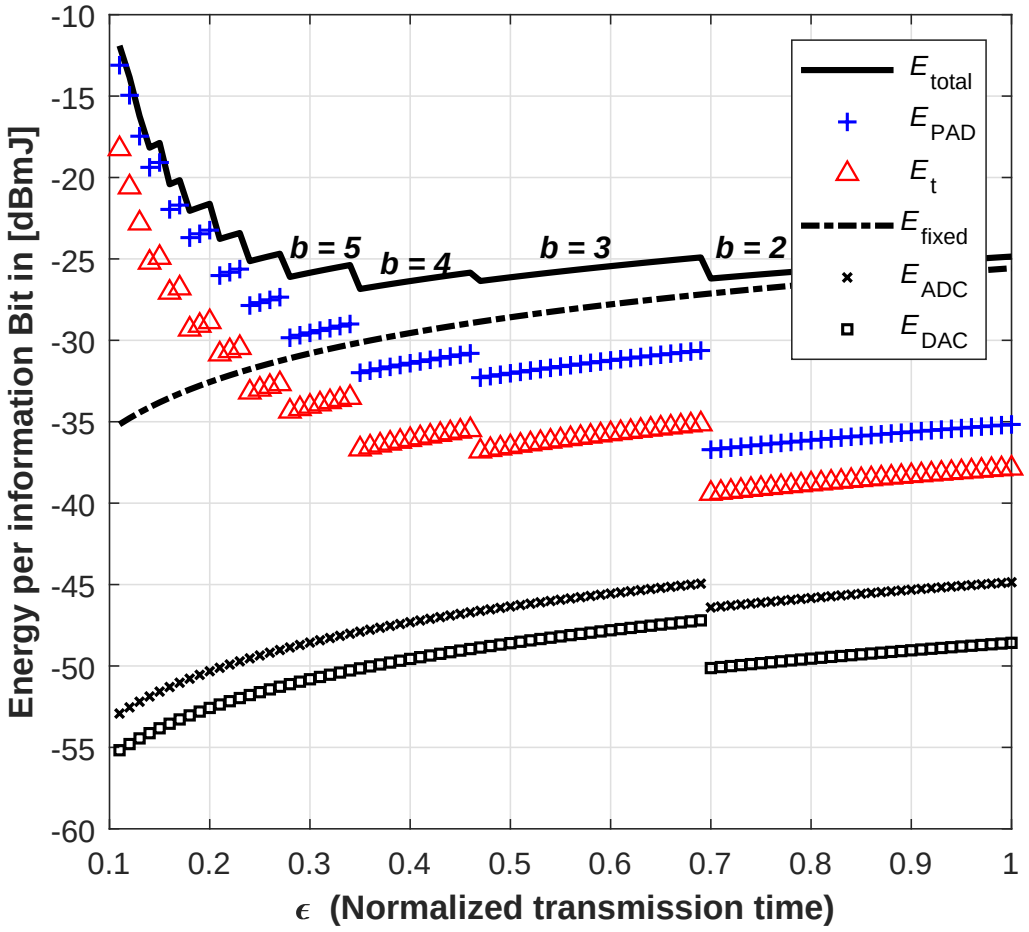

Figure 2.11: All energies for $d = 10$ m.

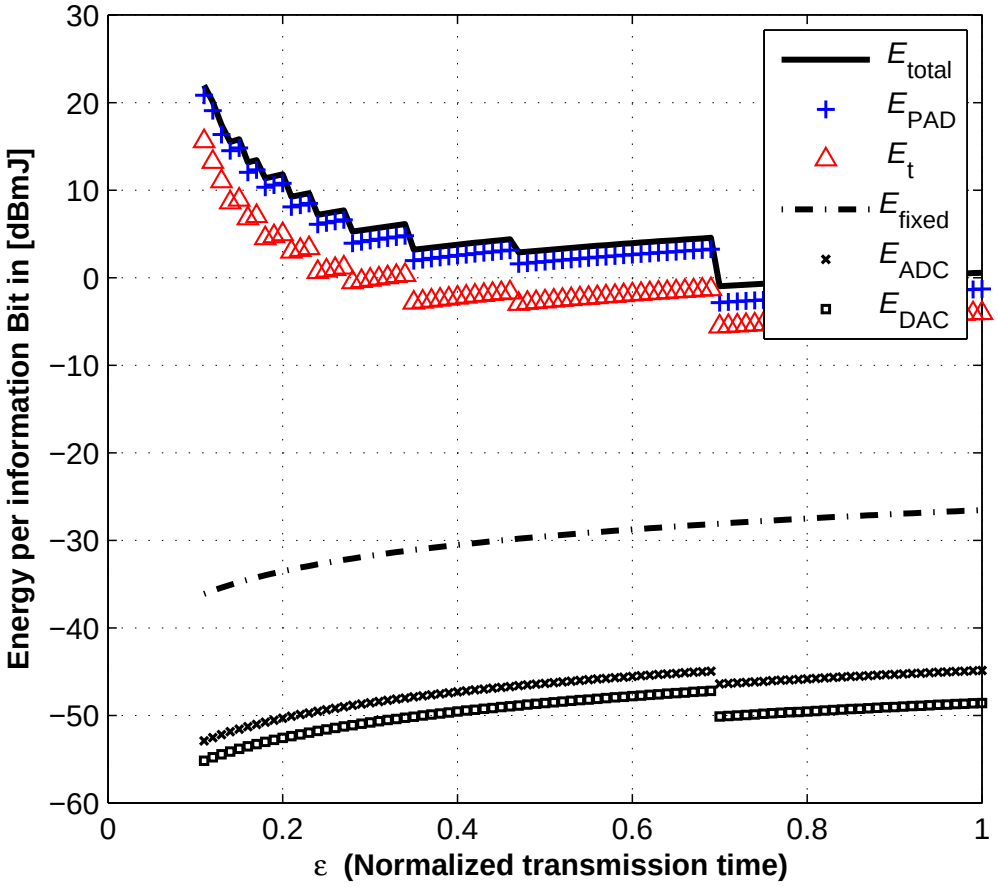

Figure 2.12: All energies for $d = 200$ m.

decreasing, as discussed earlier in Figure 2.2. E_{fixed} grows proportionally with ε. In both figures, we observe the optimum modulation order b, which is optimal in the sense of minimizing the total energy consumption per information bit in the transceiver.

Figure 2.11 considers a shorter distance of $d = 10$ m, which is applicable in wireless sensor networks, Wi-Fi, internet of things, or some small cell systems (e.g. femtocell). Figure 2.11 shows the required E_{t} and E_{PAD} are relatively small compared to E_{fixed}, which dominates the total energy consumption as ε increases and b decreases. This result agrees with the $d = 10$ m curve in Figure 2.10. In Figure 2.11, the minimum total energy occurs at $\varepsilon \approx 0.37$. Other works have observed an optimum energy consumption point similar to Cui [6,7]; however, our results in Figure 2.11 provide the following additional insights: (i) the optimum modulation order in this particular scenario is identified as $b = 4$ at (16-QAM), which is associated with $\varepsilon \approx 0.37$, (ii) energy consumption is separated into many factors, which makes it possible to precisely identify the dominant energy consumer in each scenario.

Figure 2.12 considers a longer distance of $d = 200$ m and shows that E_{t} and E_{PAD} dominate the total energy consumption for all modulation orders. Here the optimum modulation order for minimizing E_{total} is $b = 2$ (QPSK) at $\varepsilon \approx 0.70$. Again, this result agrees with the curves in Figure 2.10 for $d > 25$ m. E_{t} in Figure 2.12 is exactly that of Figure 2.2.

In both figures, because E_{DAC} and E_{ADC} are so small,[9] there are no further insights to be gained by subdividing E_{others} any more; it is better to focus on the PA parameters. These two energies are generally increasing with ε. They both shift downward at the point where $b = 2$ occurs, because the required value of N_{DAC} changes from 8 to 7.

[9]This provides enough justification for our approximation in (2.31) as $Q \approx P_{\text{fixed}}$.

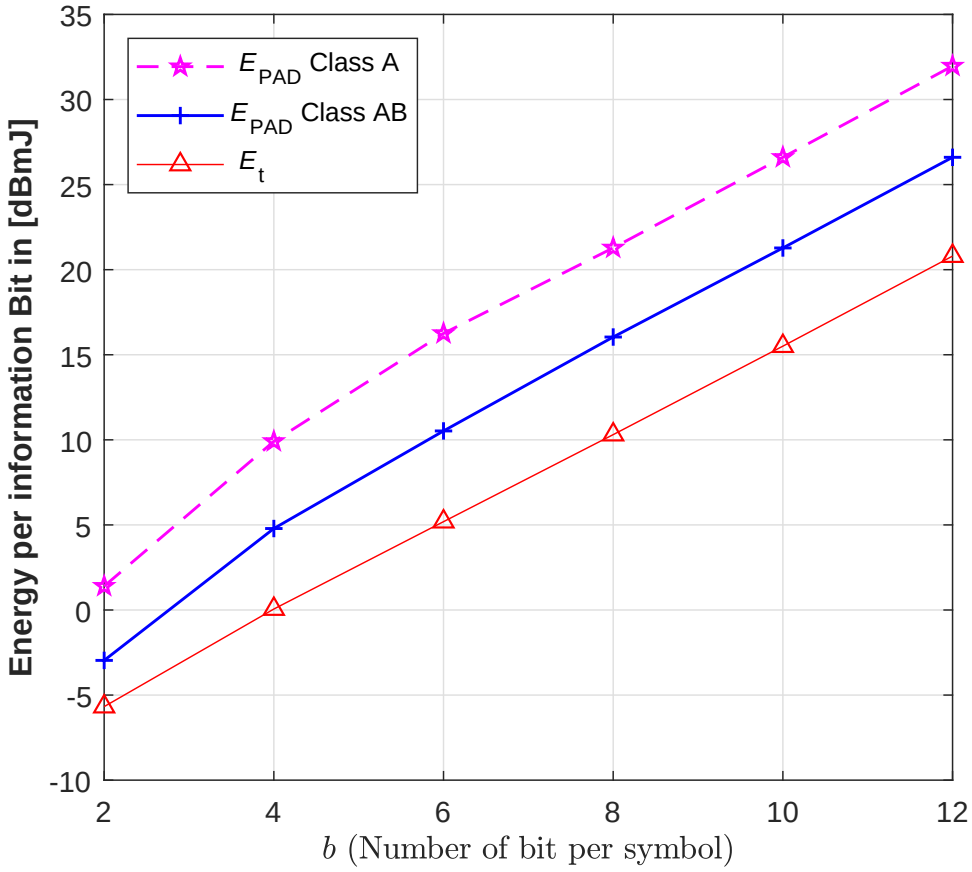

Figure 2.13: Total energy for class A and class AB PAs for $d = 200$ m.

2.6.3 The Impact of PA Class

Figure 2.13 shows that class AB PAs can achieve lower energy consumption than class A PAs, with an advantage of around 4 to 5 dB. This is because class AB PAs have a higher drain efficiency and slower decay with power back-off/PAR, as described in Eqs. (2.17) and (2.18). The values of $\mathrm{PAR}(b, 0.42)$ vs. modulation order are listed in Figure 2.5.

With the results in Figure 2.13 the remaining concern is: can the linear range of class AB PAs—which is smaller than that of class A PAs—satisfy the required power back-off of higher modulation orders? As Figure 2.5 and Table 2.3 show, $\mathrm{PAR}_{\mathrm{Mod}}(b)$ converges to around 3, i.e., 4.5 dB and the overall PAR converges to 7 dB for high modulation orders, and thus the amount of PA back-off does not become arbitrarily large. Therefore, class AB PAs can be considered a good design choice for MQAM signals with wireless mobile handsets.

2.7 Chapter Summary

In this chapter, we have developed an advanced energy consumption model for wireless cellular systems that takes into account a broad range of parameters such as PA type and efficiency, modulation order, normalized transmission time, roll-off factor of SRRC pulse, fading impact, transmission distance, and other circuit elements beyond the PA. A central idea is to separate PA energy consumption into transmitted energy and waste (heat) energy, which allows our model to give design insights that were not possible with previous energy consumption models. Through this separation, our model is able to clearly identify the impact of modulation order on the transmitted energy via the probability of error formula, and on the dissipated energy via the amount of power back-off that occurs to avoid distortion. Similarly, the model able to identify the impact

of roll-off factor on transmitted energy via the required bandwidth and on the dissipated energy via the PAR of SRRC. The results show that class AB PAs can be a good design choice even for high order MQAM modulations, because the PAR converges to 7 dB and that keeps the amount of power back-off from becoming arbitrarily large. We are also able to identify the optimal modulation order in terms of energy-efficiency in different situations, such as transceiver distances, PA classes and efficiencies, and pulse shape.

Chapter 3

Power Control

3.1 Key Points of the Chapter

- Model the impact of power control on energy consumption in which we determine the influence of transmission distance d on PA efficiency, which is similar to the impact of modulation order b via peak-to-average-power ratio (PAR), as discussed in Chapter 2.
- Jointly model the impact of power control and PAR on PA efficiency and the total energy consumption.
- Provide various approaches for mitigating/utilizing the impact of power control based on the joint model.

3.2 Motivation

Power control, as seen in Figure 3.1, is a technical mechanism that can be used to achieve better wireless system performance via a dynamic adjustment to the transmitted power. Historically, it

has been necessary for cellular systems since the early days of wireless communication. In the third generation (3G) wireless communication systems, power control played the critical role of mitigating the near–far problem, in which a strong signal from a nearby handset could make it more difficult for the base station receiver to detect/process other signals, and hence, reduce the number of user in the system [14, 15]. Currently, in the fourth generation (4G) wireless communication systems, there are even no mandatory requirements as those in 3G, power control can be utilized to reduce noise at the receiver. In some new technology of the fifth generation (5G) wireless communication systems, such as the non-orthogonal multiple access (NOMA) [16, 17], power control management will play a critical role again. In the NOMA system, which is a method for providing multiple access routes to different handsets through assigning various power levels, power control will not only mitigate interference, it will also support the multiple access scenario.

Because reducing power can save some transmitted energy, it can also reduce the PA efficiency (backing-off), resulting in a higher PA dissipated energy. Recently, an approach called *envelope tracking* has been implemented in an attempt to lessen the impact of power control on PA efficiency by continuously adjusting the supply voltage of the PA [69]. However, this approach has proven to enhance the efficiency only up to 30% [70–72], and it requires a wide-bandwidth supply and an extra processing. Therefore, power control requires further analyses to be more efficient.

For more realistic results, we jointly modeled power control and PAR. The following is a list of different types of PAR:

- PAR of multilevel quadrature amplitude modulation (MQAM). This occurs due to amplitude fluctuations in the modulated signal and due to the Nyquist pulses used in the modulation. This case has been thoroughly discussed in Chapter 2.

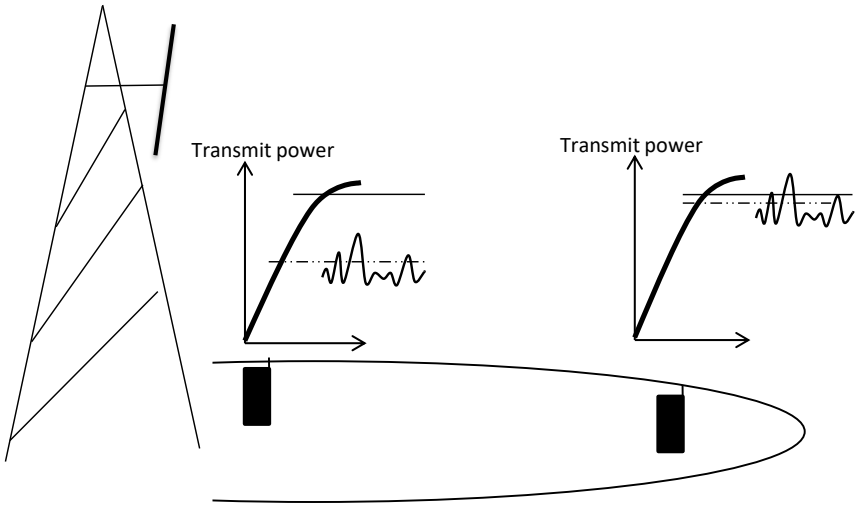

Figure 3.1: Impact of power control on PAs output power.

- PAR of orthogonal frequency division multiplexing (OFDM). Even though OFDM provides a robust solution for mitigating the impact of frequency selective fading, it requires high energy due to having high PAR. It sends data over orthogonal sub-carriers that have smaller bandwidth than the coherent bandwidth of the channel, which mitigates the inter-symbol interference. Such a system is beneficial for dense urban areas where coherent bandwidth is usually narrow. However, maintaining high PAR, typically within the range of $10 - 12$ dB [73], is difficult for OFDM in the PA. To avoid the problem of wireless handsets consuming too much energy, OFDM is currently used in the downlink side because base stations' transmitter can better handle this loss of energy [74]. However, in our quest to save energy, we are not using OFDM to its full potential to combat the uplink interference. To solve this problem, it is our goal to study power control jointly with PAR to find a more efficient way to use OFDM, especially in dense urban areas, without consuming extra energy.

As PAR represents the impact of the *system level* and power control represents the impact of the *network level* on PAs energy consumption, studying these two aspects together can help us to better understand the energy consumption of PAs and create new approaches that mitigate/utilize the impact of power control.

3.3 Power Control Analysis

We can model the total energy consumption of power control as a function of d. Whereas d can simultaneously impact the transmitted energy, E_{t}, via propagation loss and can impact PA efficiency δ via power control. Similar to Equation (2.19), where δ is modeled as a function of PAR and b, we model δ as a function of power control and d for a fixed modulation order b as

$$\delta(d) = \frac{\eta_{\max}}{\left(P_{\max}/P_{\mathrm{t}}(d)\right)^{\lambda}} , \tag{3.1}$$

where the value of maximum drain efficiency $\eta_{\max}$ and decay rate λ for various types of PAs are listed in Table 2.2. $P_{\mathrm{t}}(d)$ is the transmitted power as in Equation (2.13) at the transmission distance d. $P_{\max}$ represents the maximum output power from the PA at the maximum distance of the handset from the base station $d = d_{\max}$, i.e., $P_{\mathrm{t}}(d_{\max}) = P_{\max}$, which yields a PA efficiency of $\delta(d_{\max}) = \eta_{\max}$.

According to Model (3.1), shown in Figure 3.2, PA efficiencies as a function of transmission distance d for class A, i.e.,$\eta_{\max} = 0.35$ and $\lambda = 1$, and class AB PAs , i.e.,$\eta_{\max} = 0.55$ and $\lambda = 0.6$, when $P_{\max} = 30$ dBm at $d_{\max} = 400$ m are considered. The figure clearly shows the efficiency of class AB PAs have better performance than class A PAs with d, due to having higher maximum

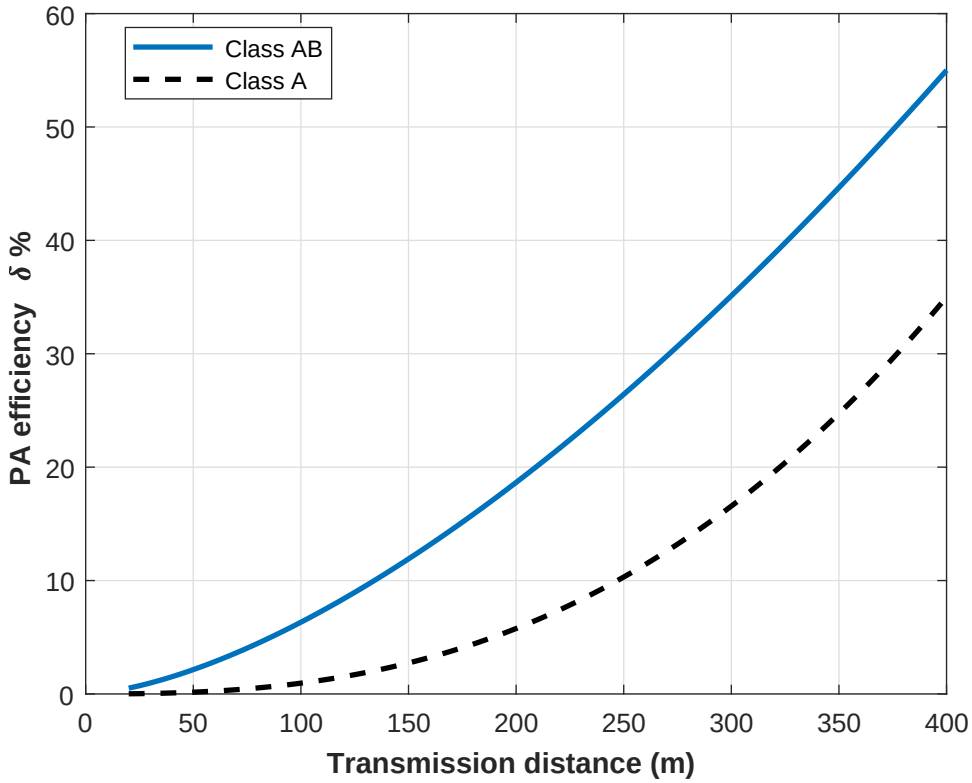

Figure 3.2: Typical PA efficiency as a function of distance for class A and class AB PAs.

drain efficiency and decreases in a slower rate.

3.4 Power Control vs. PAR of the MQAM Signal

With regard to the MQAM signal, determining the impact of the PAR and power control jointly will provide result in a more realistic model of δ. As the values of PAR and power control may fluctuate in the system (depending on the required spectral efficiency, i.e., b, and the position of the handset with respect to the base station, i.e., distance d), the PA is required to power back-off corresponding with whichever one has the maximum value. The model of δ, based on Equation (3.1) and (2.16),

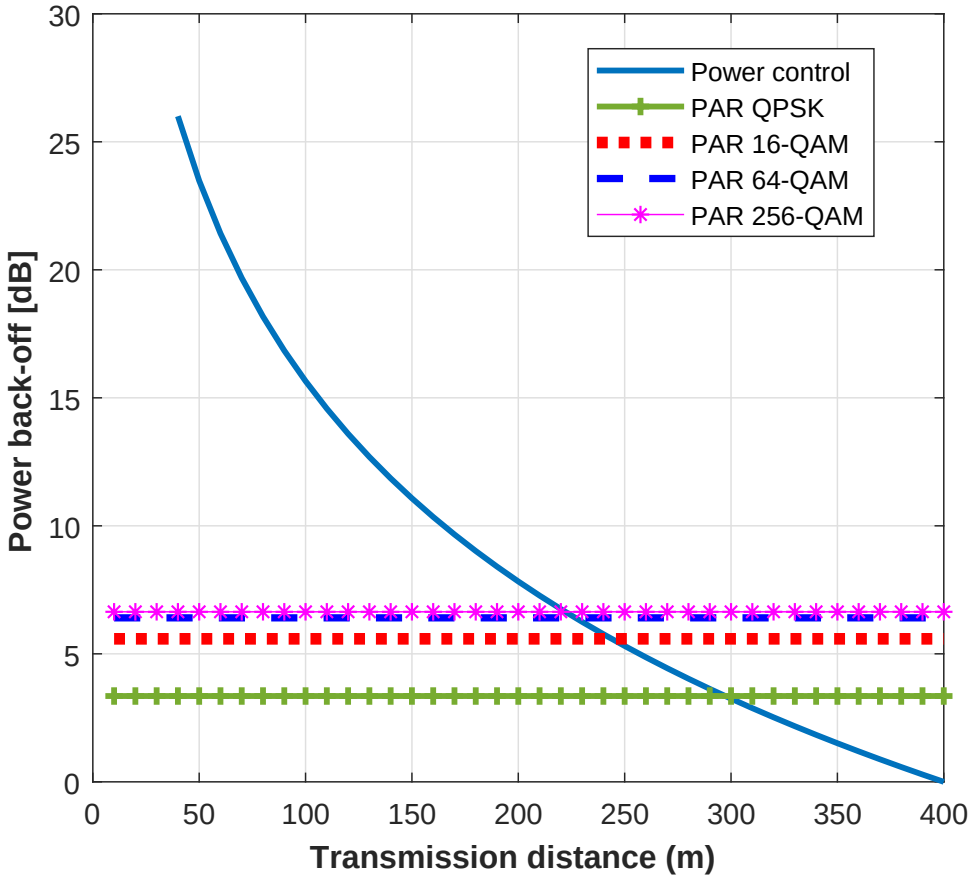

Figure 3.3: Power back-off due to power control and PAR.

can be expressed in the equation below:

$$\delta(b,d) = \frac{\eta_{\max}}{\Big(\max\{\mathrm{PAR}(b), P_{\max}/P_{\mathrm{t}}(d)\}\Big)^{\lambda}}. \tag{3.2}$$

Figure 3.3 shows the required power back-off versus the transmission distance d from 10 m up to $d_{\max}$, at various modulations[1] $b = 2,4,6,8$. At the edge of the cell (shown on the right-hand side of the figure) $d = d_{\max}$, power control is no longer necessary because it is at its maximum $P_{\mathrm{t}}(d_{\max}) = P_{\max}$, i.e., the power back-off: $P_{\max}/P_{\mathrm{t}}(d) = P_{\max}/P_{\mathrm{t}}(d_{\max}) = 0$ dB. Yet, the PA must back-off the power level to satisfy PAR. As the handset gets closer to the base station (shown on the left-hand side of the figure) the power control gradually increases as the distance decreases. The maximum power control in our example reached 25 dB, which is within the range of 25 to 30 dB listed in the literature, cf. [75, 76]. We hypothesize that the crossing points of the PAR lines and the power control line, shown in Figure 3.3, will be $d = 220$ m for $b = 8$ and $b = 6$, and $d = 300$ m for $b = 2$. In general, all the parameters within the PAR and power control region, such as the bandwidth, the probability of error, and the propagation factor, can affect the location of these points. Figure 3.4 shows the transmitted and dissipated energy as a function of d for classes A and AB PAs at $b = 6$. According to Model (3.2), at $d = 220$ m, which is the crossing point for the power control and the PAR of $b = 6$, the slopes of dissipated energy lines change. When d is greater than 220 m, the dissipated energy is affected by power control. When d is greater, the dissipated energy follows the transmitted energy.

- For the first slope when $d < 220$ m, as power control level is higher than the PAR at $b = 6$,

[1] We see that PAR is converging to 7 dB, which matches our results in Chapter 2.

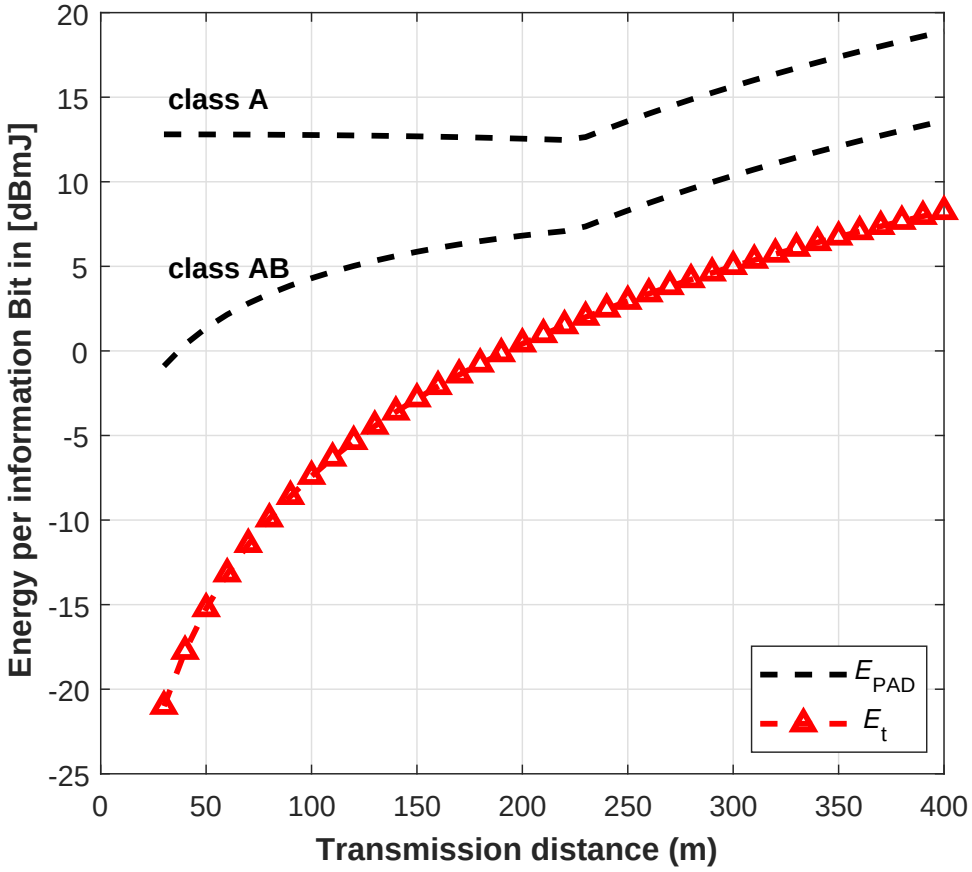

Figure 3.4: Total energy of PA with power control and PAR for 64-QAM.

Model (3.2) becomes

$$\delta(b,d) = \frac{\eta_{\max}}{\left(P_{\max}/P_{\mathrm{t}}(d)\right)^{\lambda}}. \tag{3.3}$$

The formula of dissipated energy, as shown in (2.7) can be stated as

$$E_{\mathrm{PAD}} = \frac{E_{\mathrm{t}}}{\delta} - E_{\mathrm{t}} = \frac{\left(P_{\max}/P_{\mathrm{t}}(d)\right)^{\lambda}}{\eta_{\max}} P_{\mathrm{t}}(d) T_{\mathrm{on}} - E_{\mathrm{t}}(d) = \frac{{P_{\max}}^{\lambda} \cdot \left(P_{\mathrm{t}}(d)\right)^{1-\lambda} T_{\mathrm{on}}}{\eta_{\max}} - E_{\mathrm{t}}(d), \tag{3.4}$$

where the transmitted energy $E_{\mathrm{t}}(d) = P_{\mathrm{t}}(d)T_{\mathrm{on}}$ is illustrated in Equation (2.7) as a fixed value of b. The value of T_{on} can be determined according to Equation(2.2). For class A PAs, ($\eta_{\max} = 0.35$ and $\lambda = 1$), the dissipated energy becomes

$$E_{\mathrm{PAD}} = P_{\max} T_{\mathrm{on}}/0.35 - E_{\mathrm{t}}(d) \quad : \text{class A PA}. \tag{3.5}$$

This dissipated energy remains at a high rate and is nearly fixed with d, which can be seen in Figure 3.4 on the left side of $d = 220$ m. Because the value of $E_{\mathrm{t}}(d)$ in Equation (3.5) is lessened along with d, compared to $P_{\max} T_{\mathrm{on}}/0.35$, we can notice a slight decrease in the curve as d increases. On the other hand, for class AB PAs ($\eta_{\max} = 0.55$, and $\lambda = 0.6$), the dissipated energy becomes

$$E_{\mathrm{PAD}} = {P_{\max}}^{0.6} \cdot \left(P_{\mathrm{t}}(d)\right)^{0.4} T_{\mathrm{on}}/0.55 - E_{\mathrm{t}}(d) \quad : \text{class AB PA}, \tag{3.6}$$

which provides more efficient energy performance compared to class A PA due to higher maximum drain efficiency and slower decay rate of class AB PAs, as seen in Figure 3.4.

- For the second slope when $d \geq 220$ m, as PAR is higher than the value of the power control,

Model (3.2) becomes

$$\delta(b,d) = \frac{\eta_{\max}}{\big(\mathrm{PAR}(b)\big)^{\lambda}}. \tag{3.7}$$

Hence, for fixed $b = 6$ the dissipated energy follows only the value $E_{\mathrm{t}}(d)$ for both classes of PAs:

$$E_{\mathrm{PAD}} = \frac{E_{\mathrm{t}}}{\delta} - E_{\mathrm{t}} = \frac{\big(\mathrm{PAR}\big)^{\lambda}}{\eta_{\max}} E_{\mathrm{t}}(d) - E_{\mathrm{t}}(d). \tag{3.8}$$

Generally, for different parameters of b, $d_{\max}$, $P_{\max}$, etc., the above formulas will follow the same trend; however, the crossing point position $d = 220$ m may change.

□

To sum up, as power control requires higher energy consumption in PAs, which must be appropriately addressed near base station, several approaches for mitigating the impact of power control on the PA or finding a way to better utilize it will be discussed. These approaches are bandwidth adjustment and adaptive modulation.

3.4.1 Addressing the Impact of Power Control: Bandwidth Adjustment

The bandwidth adjustments approach can be used to modify power control by spreading the transmitted power over a higher bandwidth spectrum as the handset is moving toward the base station instead of decreasing the power (backing-off). This approach can mitigate the power control issue and also increase the bit rate. However, due to the current limitations of the RF spectrum, this approach may not be feasible. The millimeter wave (mmWave) technique used in the 5G, which provides higher bandwidth [77], can be utilized as a solution to this problem. However, the intended high-frequency band for this technique raises other issues mostly related to propagation loss and PA design flaws, which is beyond the scope of this study.

3.4.2 Addressing the Impact of Power Control: Adaptive Modulation

In this approach, instead of reducing the level of power back-off in the PA, we propose to utilize the low efficiency of power control to increase the spectral efficiency. We can achieve this goal by using a high modulation order since the value of PAR is less than that of power control. This approach is illustrated in Figure 3.5. It is clear that the spectral efficiency increases without further power back-off, as this has already occurred via power control. This result would be difficult to observe without jointly modeling power control and PAR.

On the other hand, in this approach, increasing modulation orders lead to increase the total energy via the transmitted energy, see Equation(2.15), not the dissipated energy. Because PAR reaches no higher than 7 dB, see Figure 3.5, other techniques can also be used, such as OFDM.

3.5 Power Control vs. PAR of OFDM Signal

This approach can be used whenever the power control is higher than the value of PAR[2] of OFDM PAR_{OFDM}, which is, typically, in the range of 10 to 12 dB. Figure 3.5 also shows this approach used when power control is equal to 10 dB, i.e., when OFDM is used as the handset in a distance range of less than 170 m. As base stations are usually located in dense urban areas where coherent bandwidth is narrow and inter-symbol interference is typical, using OFDM in at closer range will be more effective.

Figure 3.6 shows a comparison of the energy used for the wireless handset with and without OFDM (the latter one is shown in Figure 3.4). It is obvious that for a distance of less than 170 m,

[2]For simplicity, we consider the value of PAR of OFDM the same with all modulation orders, as the value of PAR of (QAM/OFDM) is slightly higher than that of (QPSK/OFDM) [78].

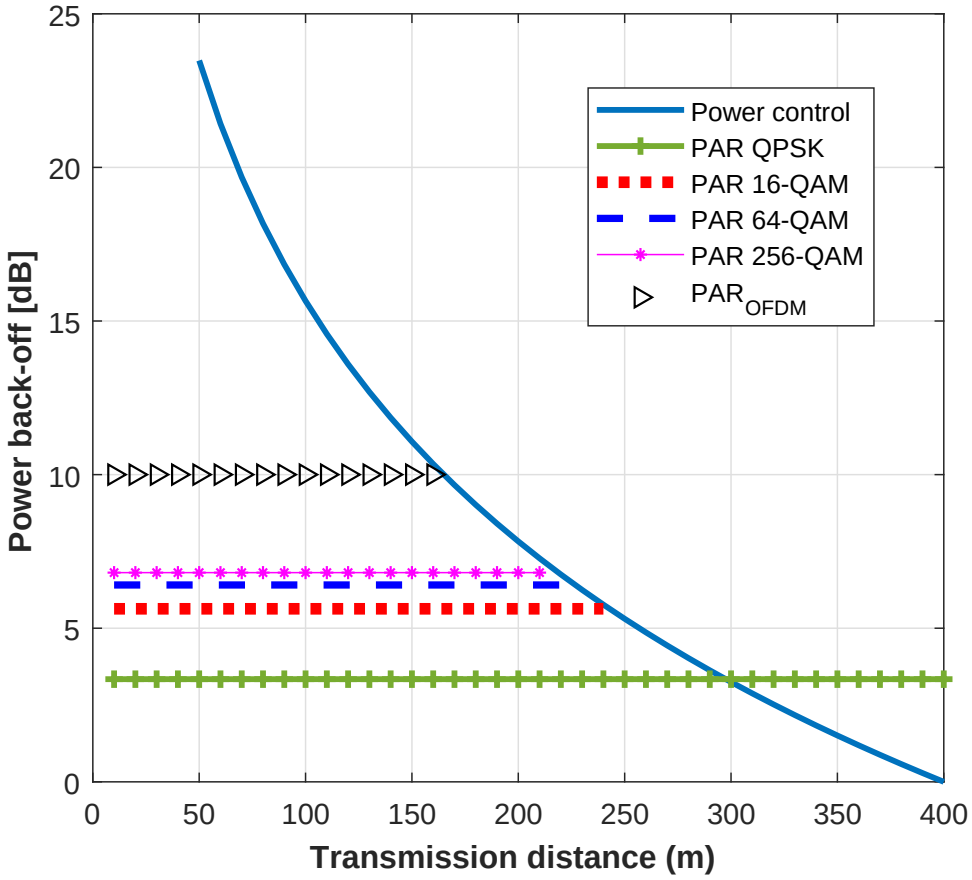

Figure 3.5: Power back-off due to power control and PAR.

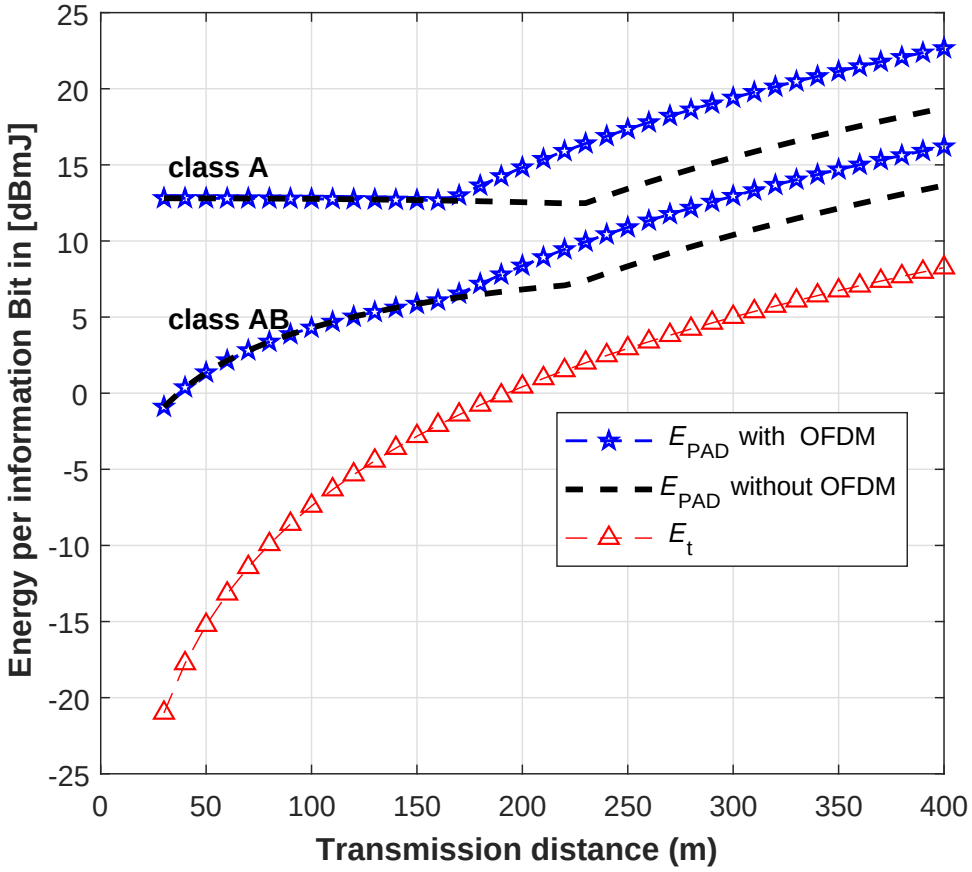

Figure 3.6: Total energy with and without OFDM for 64-QAM.

OFDM will not have any impact on the PA dissipated energy[3]. Yet, for a distance of more than 170 m, OFDM will add 4 dB of extra energy. Therefore, our approach suggests that turning OFDM off in the second scenario would be more effective.

□

After testing both the adaptive modulation and the OFDM approaches, the power control level higher than 10 dB in the range near the base station can partially be mitigated through other approaches, such as envelope tracking.

3.6 Chapter Summary

In this chapter, we developed our energy consumption model in Chapter 2 by taking into account the joint impact of power control and PAR on the energy consumption of wireless handset devices at variable ranges away from the base station. First, we modeled the power amplifier efficiency as a function of transmission distance by measuring the power back-off. Second, based the joint analysis, we proposed some approaches for best utilizing the high value of power control to obtain high spectral efficiency and/or implement OFDM without causing extra dissipated energy in the PA.

[3]OFDM may increase the transmitted energy via increasing the phase noise, but that is out of our scope.

Chapter 4

MIMO

4.1 Key Points of the Chapter

- Derive the impact of multi-antenna diversity on the transmit energy of wireless handset.
- Study and compare the bit rate with energy efficiency for multiple-input-multiple-output (MIMO) antennas. The study used MIMO as diversity and as spatial multiplexing (SM) to yield a comprehensive view of both energy-efficiency and spectral-efficiency for different situations of channel state information (CSI).
- Repeat the same comparison in the case of having massive MIMO at the base station receiver and determine the impact of that on the energy and spectral efficiency of wireless handset devices.

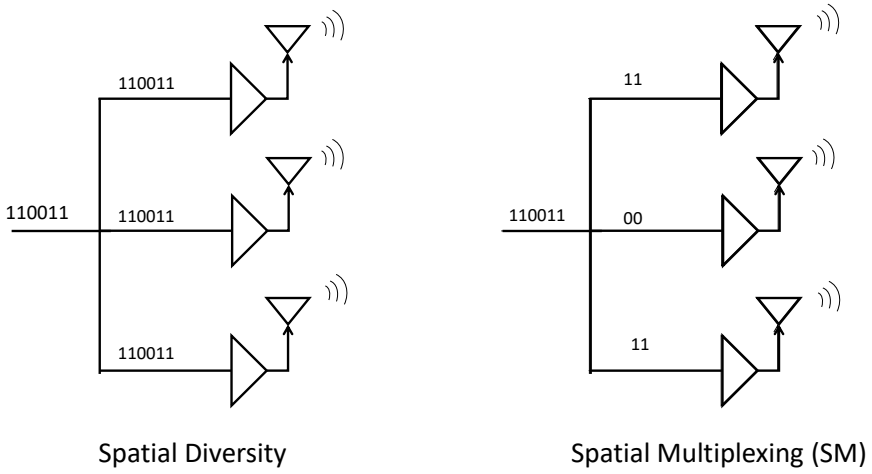

Figure 4.1: Spatial diversity vs. SM.

4.2 Motivation

MIMO becomes a very important technique for modern wireless communication systems due to the ability to increase the amount of data rate of the system via SM or due to increase the reliability of the system via spatial diversity.

Spatial diversity schemes in the transmitter and/or in the receiver can be utilized to combat fading, by sending the same information across independent fading channels. Because independent channels act differently, the impact of fading on each channel will be not the same, and that increases the probability of receiving the transmitted data correctly. In fact, diversity improves the reliability of the entire system by providing array gain and by increasing the signal to noise ratio (SNR). Modeling the impact of diversity on the energy consumption of the wireless handset is very important. SM schemes, on the other hand, have spatial channels each of which carries an independent part of the data and thus yield an increase in the total data rate of the system. Figure 4.1 shows the difference between spatial diversity and SM. For the diversity scheme, all antennas send

the same data, while for the SM scheme, each antenna sends part of the data, which is why SM provides better spectral efficiency.

Many previous works connect both diversity and SM schemes in a tradeoff [30]. The important issue of balancing the diversity–SM tradeoff in terms of energy efficiency is only recently getting the attention it deserves, cf. e.g. [26–29]. However, the energy consumption models in the previous works are built around channel capacity formulas, which in turn require that a capacity-achieving code is used, which is not always the most energy-efficient solution.

Motivated by the advantages of MIMO technique, massive MIMO is considered as one of the core techniques of the fifth generation (5G) wireless communication systems. Some of the benefits that massive MIMO can add are beam-forming, interference reduction, latency reduction, etc. [79]. However, the impact of massive MIMO antenna, at the base station, on the energy efficiency and on the bit rate performance for multi-antenna wireless handsets requires a further investigation. The works of [26, 30, 31, 80–83] provide a study of energy consumption of diversity and SM schemes for multi-antenna mobile handsets. However, each of these works has at least one of following limitations:

- They consider single antenna users [80, 81].
- They consider only conventional MIMO (up to 8×8) scenario [46, 84].
- They consider channel state information (CSI) to be always known at the transmitter [85].
- They consider only symmetric MIMO (i.e., equal numbers of antennas in the receiver and transmitter) [22].

Because massive MIMO is an important technique for next-generation communication systems,

and because CSI is difficult to obtain at the mobile handset (the transmitter), and because MIMO is not always symmetric, we provide a new study to cover all these important cases. In this Chapter, we provide an advanced energy consumption versus bit rate investigation for both diversity and SM schemes for a multi-antenna wireless handset with and without CSI in case of having only MIMO (up to 8 antennas) or massive MIMO (up to 100 antennas) at the base station.

4.3 Energy of Wireless Handsets with Multiple antennas

To understand the benefits of having multiple antennas, we study the impact of diversity on the required transmit energy in this section. As fading channel increases the required transmit energy comparing to the additive white Gaussian noise (AWGN) channel, diversity may help to reduce this energy. First, we compare the value of energy over an AWGN channel to the value of energy over a fading channel, which is derived in Chapter 2, then we derive the value of energy for different diversity orders (number of antennas as a diversity). Both the impact of receive diversity (N_{r} antennas at the base station) and transmit diversity (N_{t} antennas at the wireless handset) on the transmit energy of the wireless handset is discussed and analyzed.

4.3.1 Transmitted Energy over AWGN channel

The formula of probability of error P_{e_b} for MQAM signal over AWGN channel is [20]

$$P_{e_b} \leq W \cdot \mathrm{Q}\left(\sqrt{Z \cdot \mathrm{SNR}}\right), \tag{4.1}$$

where the W, and Z are as that in Equation (2.9). The SNR then can be stated as

$$\text{SNR} \approx \frac{1}{Z} \cdot \left(\text{Q}^{-1}\left(\frac{P_{e_b}}{W}\right) \right)^2. \tag{4.2}$$

Following the same steps of Equation (2.15), the transmit energy over AWGN channel is:

$$E_{\text{t-AWGN}} \approx \frac{1}{Z} \cdot \left(\text{Q}^{-1}\left(\frac{P_{e_b}}{W}\right) \right)^2 2B\sigma^2 N_{\text{F}}\, G(d) T_{\text{on}}. \tag{4.3}$$

The term of $\text{Q}^{-1}(P_{e_b})$ in this equation describes how low the impact of probability of error in AWGN on the transmit energy comparing to that of Rayleigh fading channel, where the energy consumption is linearly related to $1/\bar{P}_{e_b}$ as in (2.15).

The comparison between energy over AWGN channel and over Rayleigh fading channel is shown in Figure 4.2, where E_{t} of fading channel in (2.15) consumes more energy than $E_{\text{t-AWGN}}$ in (4.3) by about 18 dB for some modulation orders (for target probability of error $P_{e_b} = 10^{-3}$ and transmission distance $d = 200$ m).

4.3.2 Receiver Diversity—Transmitted Energy

For N_{r} received antennas, the received signal in each l-th antenna is

$$y_l = h_l x + w_l, \quad l = 1, \ldots, N_{\text{r}}, \tag{4.4}$$

where x is the transmitted MQAM symbol and $w \sim N(0, N_0/2)$ is AWGN, h_l is channel gain at the antenna l. At the receiver, the N_{r} received signals can be combined using various methods,

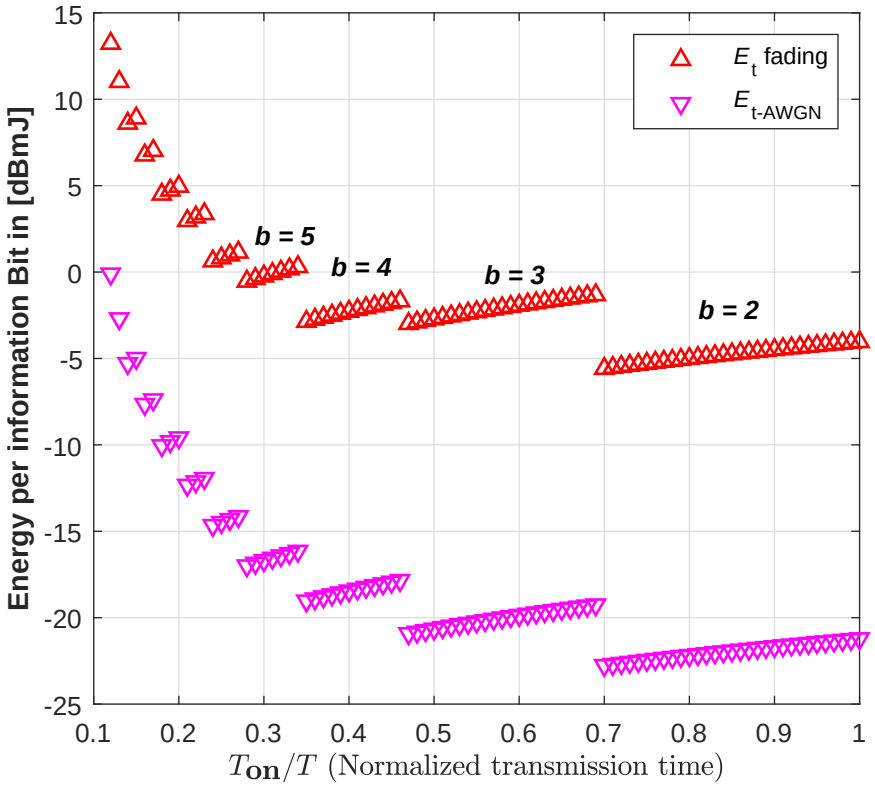

Figure 4.2: Transmitted energy for single antenna over AWGN and fading channels.

such as selection combining (SC), where the antenna with highest channel gain will be considered, and maximal ratio combining (MRC) where the antenna is weighted according to the associated channel gain to maximize the performance [20, 51, 86]. We consider MRC in this work due to its optimality [86]. Receiver diversity, using MRC, provides two types of gain: 1) diversity gain, which combats the effects of the fading; and 2) array gain, which increases the SNR as a result of receiving multiple signals through multiple antennas [51][1]. As such, the average probability of error, in Equation 2.9, becomes

$$\bar{p}_{eb} \leq W \cdot \mathbb{E}_h \left\{ \mathrm{Q}\left(\sqrt{Z \cdot \mathrm{SNR}||h||^2} \right) \right\}, \tag{4.5}$$

[1] SC has only a diversity gain.

where

$$||h||^2 = \sum_{l=1}^{N_r} |h_l|^2,$$

and SNR is the average branch signal to noise ratio and is assumed to be equal for all branches. The distribution of $||h||^2$ is Chi-squared with $2N_r$ degrees of freedom, which has the probability density function [86]

$$f(x) = \frac{1}{(N_r - 1)!} x^{N_r - 1} e^{-x}, \qquad x \geq 0 \tag{4.6}$$

The solution of (4.5) for general MQAM signals, which is derived in Appendix D, can be stated as:

$$\bar{P}_{e_b} \leq W \left(\frac{1-\mu}{2}\right)^{N_r} \sum_{l=0}^{N_r - 1} \binom{N_r - 1 + l}{l} \left(\frac{1+\mu}{2}\right)^{l}, \tag{4.7}$$

where

$$\mu = \sqrt{\frac{Z \cdot \mathrm{SNR}}{2 + Z \cdot \mathrm{SNR}}}. \tag{4.8}$$

For high SNR

$$\frac{1+\mu}{2} \approx 1, \quad \text{and} \quad \frac{1-\mu}{2} \approx \frac{1}{2\, Z \cdot \mathrm{SNR}}.$$

Furthermore, we can write

$$\sum_{l=0}^{N_r - 1} \binom{N_r - 1 + l}{l} = \binom{2N_r - 1}{N_r}.$$

Hence, Equation (4.5) can be stated as

$$\bar{P}_{e_b} \leq W \cdot \binom{2N_\mathrm{r}-1}{N_\mathrm{r}} \left(\frac{1}{2\,Z \cdot \mathrm{SNR}}\right)^{N_\mathrm{r}}. \tag{4.9}$$

Thus, the SNR at each receiver antenna is

$$\mathrm{SNR} \approx \frac{1}{2Z} \cdot \left(\frac{W}{\bar{p}_{eb}} \cdot \binom{2N_\mathrm{r}-1}{N_\mathrm{r}}\right)^{\frac{1}{N_\mathrm{r}}}. \tag{4.10}$$

This result is similar to that of [51, Eq. (7-23)], which was derived using approximations to the Q-function, and also to [86, Eq. (9-35)], which was derived using the moment-generating function. The transmitted energy in case of receiver diversity using (2.12), (2.13), and (4.10) is

$$E_{\text{t-diversiy}} \approx \frac{1}{Z} \cdot \left(\frac{W}{\bar{P}_{e_b}} \cdot \binom{2N_\mathrm{r}-1}{N_\mathrm{r}}\right)^{\frac{1}{N_\mathrm{r}}} B\sigma^2 N_f G(d) T_{\mathrm{on}} \tag{4.11}$$

The plot of this equation for different diversity orders (which is N_r here), is shown in Figure 4.3. Comparing Figure 4.3 to Figure 4.2, we see that diversity mitigates the impact of fading on the energy by exploiting the diversity and array gains of MRC. We also point out that the curve for diversity order 1, i.e., no diversity, is the same as the Rayleigh fading E_t in Figure 4.2. As N_r increases, the gap between $E_{\text{t-diversiy}}$ curves decreases. This is because the term $(\frac{1}{\bar{p}_{eb}})^{\frac{1}{N_\mathrm{r}}}$ in Equation (4.11) approaches unity. Therefore, we can say that diversity order 2 has the largest incremental gain in the formula of (4.11).

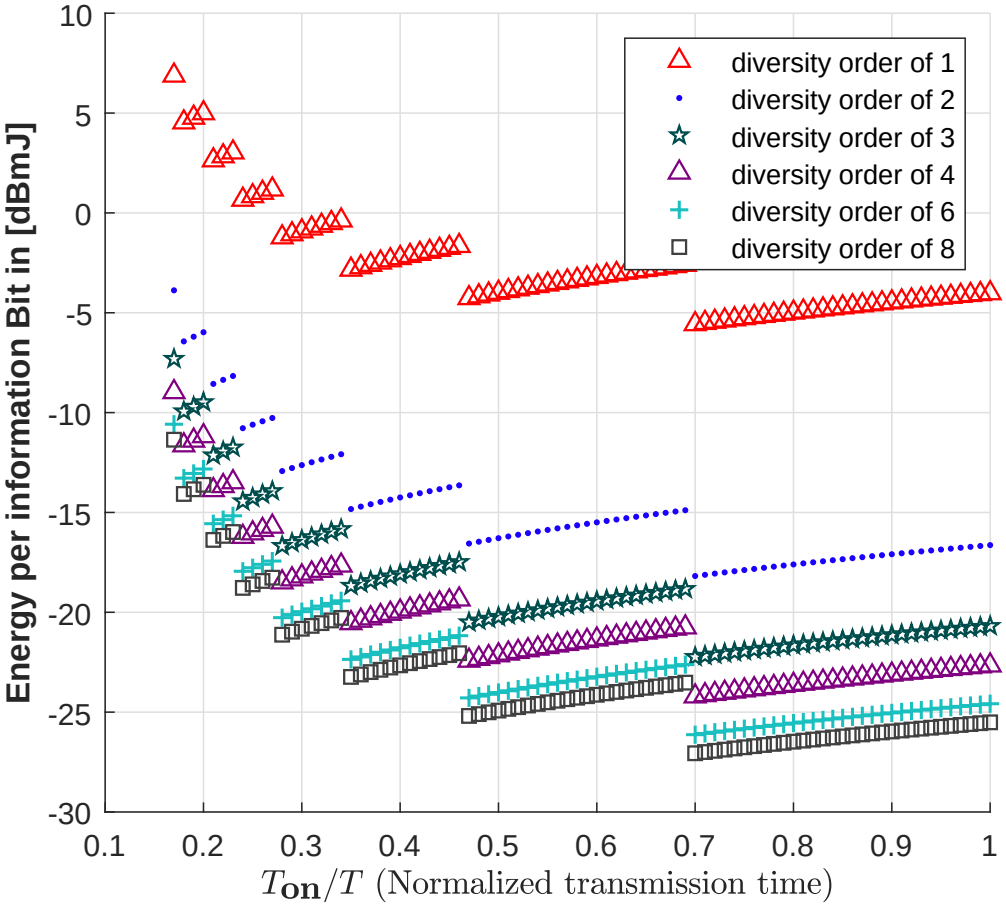

Figure 4.3: Faded transmitted energy with various diversity orders.

4.3.3 Transmit Diversity

Transmit diversity can provide the same performance of the receiver diversity under the condition of availability of channel state information [45]. If CSI is available, then transmit diversity will provide the same performance as receive diversity does in term of $E_{\text{t-diversiy}}$:

$$E_{\text{t-diversiy}} \approx \frac{1}{Z} \cdot \left(\frac{W}{\bar{P}_{e_b}} \cdot \binom{2N_{\text{t}} - 1}{N_{\text{t}}} \right)^{\frac{1}{N_{\text{t}}}} B\sigma^2 N_f G(d) T_{\text{on}} \tag{4.12}$$

Without CSI, transmit diversity should be achieved using another technique besides sending the same signal on multiple antennas (such as space-time coding [87, 88]).

4.4 MIMO

In this section, we study the impact of having multiple antennas at both the receiver and transmitter as diversity and as SM on the energy consumption of wireless handsets. The number of antennas at the base station receiver is considered to be $N_{\text{r}} = 8$, where the number of antennas at the handset is considered to be in the range $1 \leq N_{\text{t}} \leq 8$. Figure 4.4 shows an example for $N_{\text{r}} = 8$ and $N_{\text{t}} = 3$, where the case of having one antenna has been discussed in Section 4.3.2. These numbers are chosen to be realistic, as currently most of the base stations have multiple received antennas already, so we observe the impact of having extra handsets' antennas on the energy consumption of that handset via diversity or via SM, as SM requires multiple antennas on both sides.

We consider two cases for CSI: (1) CSI is known at both the transmitter and receiver (CSIT+R), and (2) CSI is known at the receiver only (CSIR). The channel is considered to be an independent and identically distributed (i.i.d) MIMO Rayleigh fading with full rank of $r = \min(N_{\text{t}}, N_{\text{r}}) = N_{\text{t}}$,

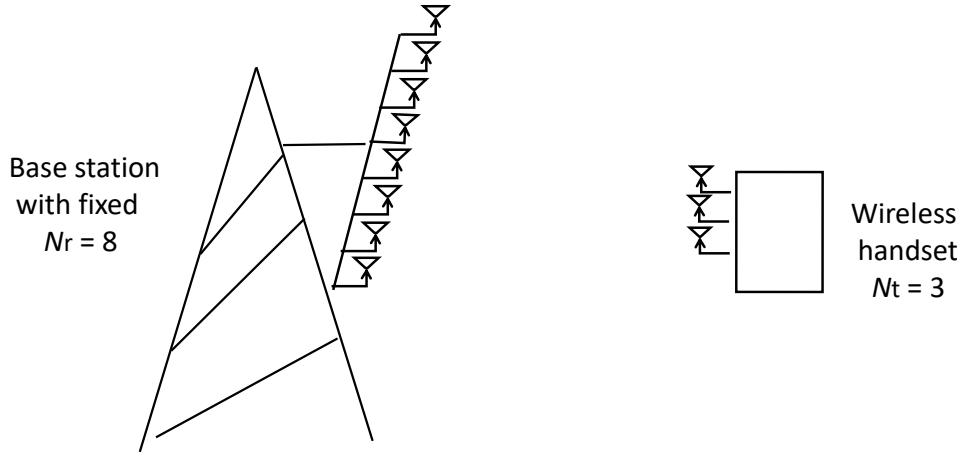

Figure 4.4: MIMO scheme as $N_t = 3$ and the number of receive antennas is fixed at $N_r = 8$.

due to $N_t \leq N_r$.

Diversity and SM are now discussed for CSIT+R and CSIR in the following subsections:

1. *MIMO Spatial Diversity with CSIT+R*

2. *MIMO Spatial Diversity with CSIR*

3. *MIMO Spatial Multiplexing with CSIT+R*

4. *MIMO Spatial Multiplexing with CSIR*

where the energy in each subsection is labeled with one of the numerals 1, 2, 3, and 4, from the respective subsection.

4.4.1 MIMO Spatial Diversity with CSIT+R

For known CSI, the transmitter can provide array and diversity gains, similar to that of MRC receiver diversity [45]. From (4.11), the generalized transmit power of MIMO with N_t and N_r

diversity gain is

$$P_{\text{t-A}} \approx \frac{1}{Z} \cdot \left(\frac{W}{\bar{p}_{eb}} \right)^{\frac{1}{N_t N_r}} B\sigma^2 N_F G_d. \tag{4.13}$$

The diversity gain for the example in Figure 4.4 is equal to 3×8. The transmitted energy for each antenna is

$$E_{\text{t-A}} = \frac{1}{N_t} P_{\text{t-A}} T_{\text{on}} = \frac{1}{N_t} P_{\text{t-A}} \frac{L}{R_s b}, \tag{4.14}$$

where T_{on} is defined in (2.3). The factor of $\frac{1}{N_t}$ is the transmitter array gain. The total energy consumption in MIMO case is the addition of the PA energy (transmitted E_t and dissipate E_{PAD}) on each antenna and the other circuits' energy E_{others} as

$$E_{\text{total-A}} = \sum^{N_t} (E_{\text{t-A}} + E_{\text{PAD}} + E_{\text{others}}) = \sum^{N_t} (\frac{1}{N_t} P_{\text{t-A}} \frac{L}{R_s b} + E_{\text{PAD}} + E_{\text{others}}), \tag{4.15}$$

where E_{PAD} and E_{others} are well defined in Chapter 2. However, E_{others} in this chapter, only the other energy in the handset transmitter. Figure 4.5 plots the total energy consumption as a function of N_t for fixed $N_r = 8$, and equal energy on each transmit antenna. Additional implications of Figure 4.5 are discussed in Section 4.6.

The transmitter array and diversity gains are not available without CSI. However, some techniques, such as space-time coding [87, 88], can be utilized to obtain the diversity gain, as discussed next.

4.4.2 MIMO Spatial Diversity with CSIR

As we pointed out, there is no diversity or array gain in the transmitter without CSI. However, the Alamouti approach [87] of space-time coding with 2×2, and later the Jafarkhani approach [88,

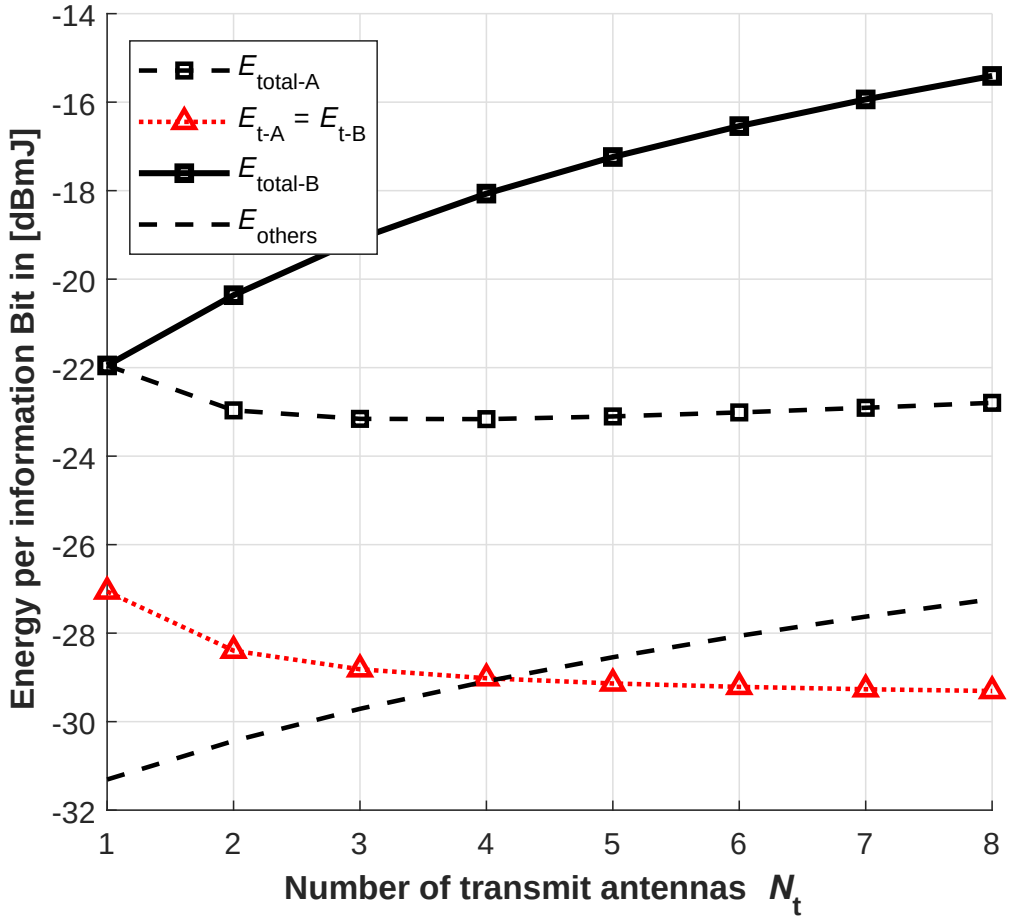

Figure 4.5: Energy consumption of MIMO diversity CSIT+R with $E_{\text{total-A}}$ and CSIR with $E_{\text{total-B}}$ vs. N_{t}, for $N_{\text{r}} = 8$. On the left-hand side we have N_{t} x N_{r}, i.e., 1 x 8 diversity gain, on the right-hand side we have 8 x 8 diversity gain.

Chapter 4] with 4×4 and 8×8 code matrices, are utilized to obtain a diversity gain of $N_t N_r$. The transmit power is similar to Equation (4.13), and is

$$P_{\text{t-B}} \approx \frac{1}{Z} \cdot \left(\frac{W}{\bar{p}_{eb}} \right)^{\frac{1}{N_t N_r}} B\sigma^2 N_F G_d. \tag{4.16}$$

Further, for the space-time coding technique, N_t different signals are conveyed over N_t time steps, i.e., the bit rate and the transmit time are both increased by N_t,

$$T_{\text{on}} \geq \frac{L}{R_s b N_t} N_t = \frac{L}{R_s b}. \tag{4.17}$$

However, space-time coding does not yield an array gain [88], i.e., the transmitted energy is

$$E_{\text{t-B}} = P_{\text{t-B}} T_{\text{on}} = P_{\text{t-B}} \frac{L}{R_s b}. \tag{4.18}$$

Then the total energy consumption increases linearly with N_t as

$$E_{\text{total-B}} = \sum^{N_t} (P_{\text{t-B}} \frac{L}{R_s b} + E_{\text{PAD}} + E_{\text{others}}). \tag{4.19}$$

Figure 4.5 plots the spatial diversity energy consumption in the case of CSIR. It shows that although $E_{\text{t-B}}$ decreases with increasing N_t, the total energy, $E_{\text{total-B}}$, begins to increase due to the absence of array gain.

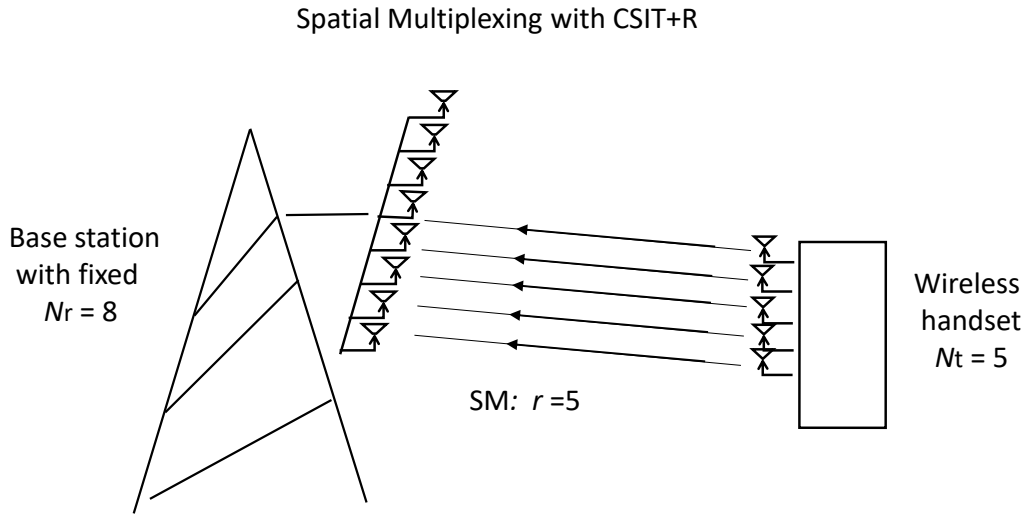

Figure 4.6: Spatial Multiplexing for $r = 5$ with CSIT+R.

4.4.3 MIMO Spatial Multiplexing with CSIT+R

In the SM scheme, for known CSI and for a full rank channel (i.i.d), the transmitted data can be split into r independent sub-streams with a process called *eigenbeamforming* [45,51]. This process exploits the CSI at the transmitter to maximize channel usage through a power allocation approach called *waterfilling*, where the transmit power for each channel depends on the gain of that channel. The total bit rate of eigenbeamforming is $\sum^{r}(R_s b)_i$, where $(R_s b)_i$ denotes the possibility that the bit rate can vary with each substream. Figure 4.6 shows an example of SM for $r = 5$ with five eigenbeamforming sub-streams. In order to compare SM with diversity, we apply the assumption of uniform-rate-allocation, i.e., all channels have the same bit rate. The total bit rate increases linearly with r, which is the main purpose of MIMO:

$$\text{bit rate} = \sum_{i=1}^{r}(R_s b)_i = R_s b\, r. \tag{4.20}$$

Then with a full rank channel, T_{on} in (2.3) can be written as

$$T_{\text{on}} \geq \frac{L}{R_{\text{s}} b\, r}. \tag{4.21}$$

In the SM MIMO receiver, using linear decoding techniques such as zero forcing (ZF) or minimum mean squared error (MMSE), the diversity gain decreases to $(N_{\text{r}} - r + 1)$, as there is no diversity for full SM MIMO[2] ($N_{\text{r}} = N_{\text{t}}$) [90, page. 135]. The transmit power is then

$$P_{\text{t-C}} \approx \frac{1}{2Z} \cdot \left(\frac{W}{\bar{p}_{eb}} \right)^{\frac{1}{N_{\text{r}} - r + 1}} B\sigma^2 N_{\text{F}} G_d. \tag{4.22}$$

The transmitted energy is:

$$E_{\text{t-C}} = P_{\text{t-C}} T_{\text{on}} = P_{\text{t-C}} \frac{L}{R_{\text{s}} b\, r}. \tag{4.23}$$

The total energy for SM with the waterfilling algorithm is

$$E_{\text{total-C}} = \sum^{r} (P_{\text{t-C}} \frac{L}{R_{\text{s}} b\, r} + E_{\text{PAD}} + E_{\text{others}}). \tag{4.24}$$

For *high SNR*, the performance of the waterfilling allocation is considered to be the same as the equal-power-allocation scene [45]. $\frac{1}{r}$ acts here as an array gain. Notice, if we have different bit rate on each antennas, the PA energy may be different for each.

Figure 4.7 shows the total energy consumption and the bit rate versus r for a receiver diversity of $N_{\text{r}} = 8$ in the SM scheme. On the left-hand side of the figure, where $r = 1$, the diversity gain is $(N_{\text{r}} - r + 1) = 8$ and the bit rate is only $R_{\text{s}} b$. On the right-hand side, where $r = 8$, the diversity gain

[2]With full SM MIMO, only maximum likelihood (ML) detection can provide receiver diversity gain [22, 82], but it is NP-hard [89] and thus infeasible for a massive MIMO receiver, so we leave that for future work.

is $(N_r - r + 1) = 1$ and the bit rate is $8 \times R_s b$. We also notice that E_{others} is decreasing with r as the circuits are active for a shorter time $T_{on} \geq L/(R_s br)$. For the example in Figure 4.6, where $N_r = 8$ and $r = 5$, the diversity gain is $N_r - r + 1 = 3$, as only 3 antennas are remaining on the base station receiver to perform diversity. On the other hand, the transmit bit rate becomes = $5 \times R_s b$.

For *low SNR*, the transmitter will choose to transmit on the best available channel to avoid wasting energy. This means, increasing number of antennas at the transmitter N_t has no impact on bit rate, because only one antenna is utilized; the one associated with the best available channel, the rest can be used as diversity, which is similar to the case in Section 4.4.1, or go to sleep, in which the total energy becomes

$$E_{\text{total-C}} = (P_{\text{t-C}} \frac{L}{R_s b} + E_{\text{PAD}} + E_{\text{others}}). \tag{4.25}$$

4.4.4 MIMO Spatial Multiplexing with CSIR

Without CSI at the transmitter, SM can still be applied with certain techniques. The easiest and most common technique is the vertical Bell Laboratories layered space-time (VBLAST) approach [45,90], where the transmitter sends independent and equal power signals on each of the N_t antennas, regardless of the channel conditions. Similar to Equation (4.22), the transmitted power is

$$P_{\text{t-D}} \approx \frac{1}{Z} \cdot \left(\frac{W}{\bar{p}_{eb}} \right)^{\frac{1}{N_r - N_t + 1}} B\sigma^2 N_F G_d. \tag{4.26}$$

Even with the equal power allocation in VBLAST, the bit rates on each transmit antenna are not necessarily equal. Therefore, for simplicity, we assume uniform rate allocations here as well,

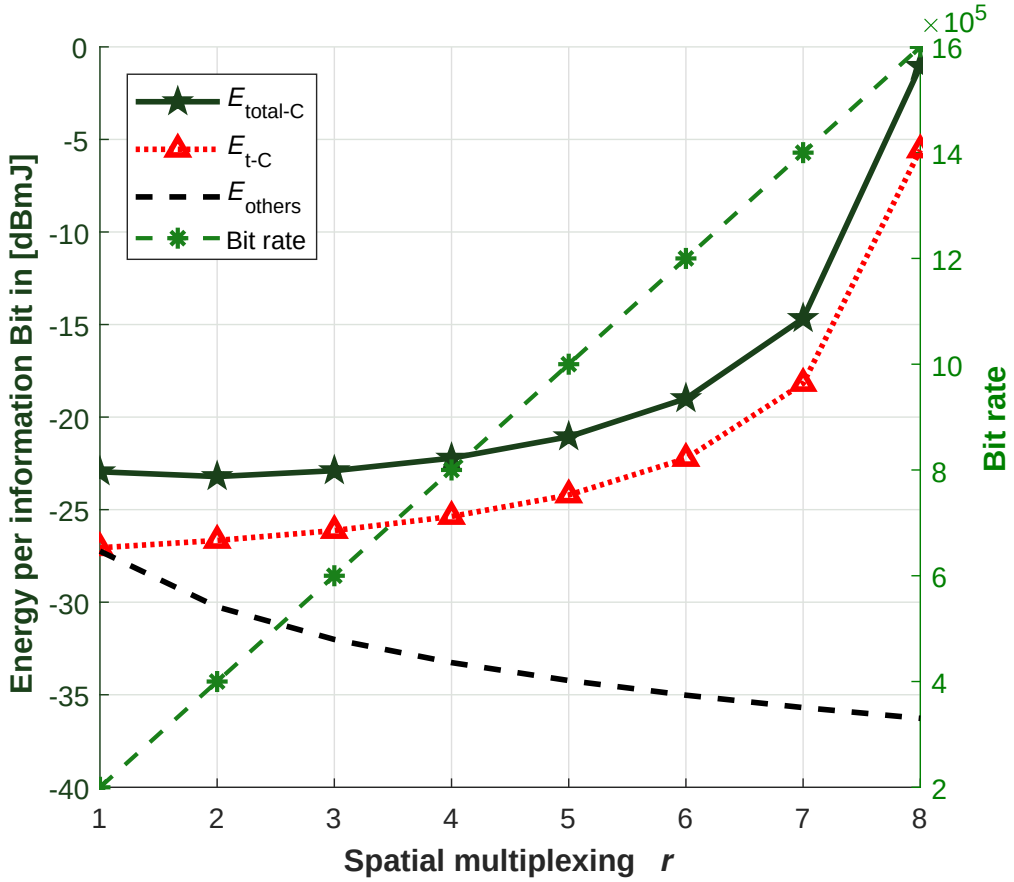

Figure 4.7: Energy consumption of MIMO spatial multiplexing SM CSIT+R vs. r, with $N_{\text{r}} = 8$. On the left-hand side, as $r = 1$, we have a diversity gain of 1 x 8. On the right-hand side, as $r = 8$, we have full spatial multiplexing, no diversity gain.

$R_s b N_t$, and hence

$$T_{\text{on}} \geq \frac{L}{R_s b N_t}. \tag{4.27}$$

The transmit energy is

$$E_{\text{t-D}} = P_{\text{t-D}} T_{\text{on}} = P_{\text{t-D}} \frac{L}{R_s b\, N_t}. \tag{4.28}$$

For VBLAST, the total energy is

$$E_{\text{total-D}} = \sum^{N_t} (P_{\text{t-D}} \frac{L}{R_s b\, N_t} + E_{\text{PAD}} + E_{\text{others}}). \tag{4.29}$$

These equations look similar to those of SM with CSIT+R at high SNR. However, the reliability of VBLAST is less than that of eigenbeamforming [45], which may require some additional steps, such as re-transmission, where the amount of energy can be determined by the number of re-transmission, which is beyond the scope of this work.

□

The energy consumption equations of the four subsections above are summarized in Table 4.1, where $K_2 = \frac{1}{Z} B \sigma^2 N_F G_d$, and E_{PAD} in each section follow the E_t of that section.

Table 4.1: MIMO bit rate and energy consumption.

	Diversity	SM
CSIT+R	A	C
P_t	$\left(\frac{W}{\bar{p}_{eb}}\right)^{\frac{1}{N_t N_r}} \cdot K_2$	$\left(\frac{W}{\bar{p}_{eb}}\right)^{\frac{1}{N_r - r + 1}} \cdot K_2$
T_{on}	$\frac{L}{R_s b}$	$\frac{L}{R_s b r}$
$E_{\text{total-MIMO}}$	$\sum^{N_t} (\frac{1}{N_t} P_{\text{t-A}} \frac{L}{R_s b} + E_{\text{PAD}} + E_{\text{others}})$	$\sum^{r} (P_{\text{t-C}} \frac{L}{R_s b\, r} + E_{\text{PAD}} + E_{\text{others}})$
CSIR	B	D
P_t	$\left(\frac{W}{\bar{p}_{eb}}\right)^{\frac{1}{N_t N_r}} \cdot K_2$	$\left(\frac{W}{\bar{p}_{eb}}\right)^{\frac{1}{N_r - N_t + 1}} \cdot K_2$
T_{on}	$\frac{L}{R_s b}$	$\frac{L}{R_s b N_t}$
$E_{\text{total-MIMO}}$	$\sum^{N_t} (P_{\text{t-B}} \frac{L}{R_s b} + E_{\text{PAD}} + E_{\text{others}})$	$\sum^{N_t} (P_{\text{t-D}} \frac{L}{R_s b\, N_t} + E_{\text{PAD}} + E_{\text{others}})$

Table 4.2: Massive MIMO bit rate and energy consumption.

	Diversity	SM
CSIT+R	A	C
P_t	$\left(\frac{W}{\bar{p}_{eb}}\right)^{\frac{1}{N_\mathrm{t}\infty}} \cdot K_2 = K_2$	$\left(\frac{W}{\bar{p}_{eb}}\right)^{\frac{1}{\infty - r+1}} \cdot K_2 = K_2$
bit rate	$R_\mathrm{s} b$	$R_\mathrm{s} b r$
CSIR	B	D
P_t	$\left(\frac{W}{\bar{p}_{eb}}\right)^{\frac{1}{N_\mathrm{t}\infty}} \cdot K_2 = K_2$	$\left(\frac{W}{\bar{p}_{eb}}\right)^{\frac{1}{\infty - N_\mathrm{t}+1}} \cdot K_2 = K_2$
bit rate	$R_\mathrm{s} b$	$R_\mathrm{s} b N_\mathrm{t}$

4.5 Massive MIMO

For a massive MIMO system, the large number of receive antennas in the base station—100 or more [79]—has a significant impact on the system performance including the energy consumption of the wireless handset. For massive MIMO, the starting points for the energy consumption equations are the ones from the previous section, but we are interested in the asymptotic behavior[3] of $N_\mathrm{r} \to \infty$. Hence

$$\begin{aligned} P_\mathrm{t} \approx & \frac{1}{Z} \cdot \left(\frac{W}{\bar{p}_{eb}}\right)^{\frac{1}{N_\mathrm{t}(N_\mathrm{r} \to \infty)}} B\sigma^2 N_\mathrm{F} G_d \\ \approx & \frac{1}{Z} \cdot \left(\frac{W}{\bar{p}_{eb}}\right)^{\frac{1}{(N_\mathrm{r} \to \infty) - r+1}} B\sigma^2 N_\mathrm{F} G_d \\ \approx & \frac{1}{Z} B\sigma^2 N_\mathrm{F} G_d = K_2. \end{aligned} \tag{4.30}$$

The large value of N_r provides a large diversity gain, even in the SM scheme where ZF and MMSE decoding are used. The impact of probability of error $\bar{p}_{eb}$ in the transmit power equations is normalized as $N_\mathrm{r} \to \infty$. The energy consumption equations for massive MIMO are listed in Table 4.2.

[3] In our plots on massive MIMO, we use the value of $N_\mathrm{r} = 100$.

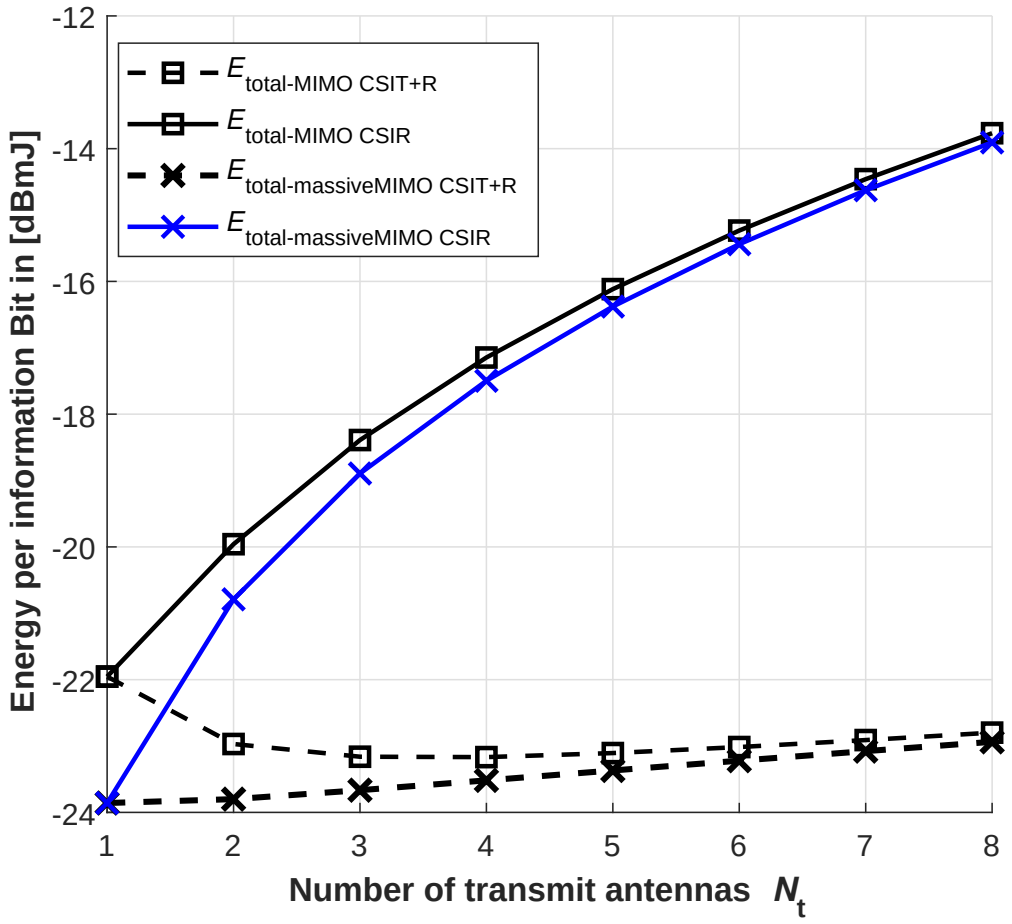

Figure 4.8: Total energy consumption per bit at the handset vs. N_t, as having $N_r = 8$ for MIMO and $N_r = 100$ for massive-MIMO using diversity scheme for both cases :CSIT+R and CSIR.

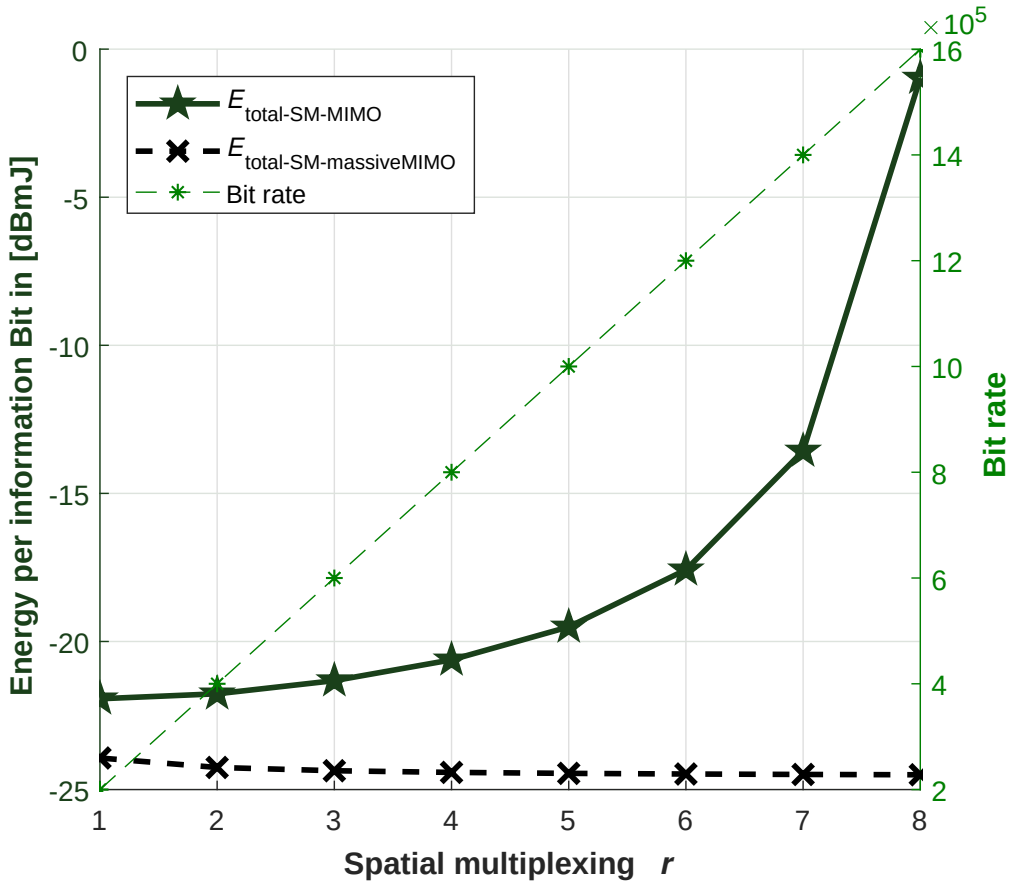

Figure 4.9: Total energy consumption per bit at the handset and the total bit rate vs. SM r, as having $N_{\text{r}} = 8$ for MIMO and $N_{\text{r}} = 100$ for massive MIMO.

4.6 Results and Discussion

Figures 4.5 and 4.7 show that the circuit energy E_{others} is much smaller than the transmit energy in a long-range communication scenario. This is because the transmit energy and power amplifier energy dominate other circuits' energies in the transceiver.

For a MIMO system, Figure 4.5 illustrates that there is little to be gained in terms of energy efficiency by increasing N_{t} at the wireless handset; these results are for a receiver diversity of $N_{\text{r}} = 8$, but in light of the diminishing incremental gains in Figure 4.3, we expect a similar result for $N_{\text{r}} \geq 4$. In fact, in the case of CSIR—which is the more common scene—Figure 4.5 shows that increasing N_{t} results in greater energy consumption $E_{\text{total-B}}$ due to the absence of array gain. Figure 4.8 shows that massive MIMO can provide a slight improvement in energy consumption over conventional MIMO for diversity schemes.

For SM, in the case of CSIT+R and for high SNR, Figure 4.7 shows that increasing N_{t} assigns additional receive antennas from diversity mode to SM mode. This increases the bit rate linearly with N_{t}, but also increases the energy consumption. The results in Figure 4.9 shows a potential solution for energy consumption in a SM scheme compared to conventional MIMO. This is because the large excess number of receive antennas provides a large diversity gain.

4.7 Chapter Summary

In this chapter, we develop our model further to study the energy and spectral efficiency for a multi-antenna wireless handset with the cases of having MIMO and massive MIMO at the base station receiver. Our research includes analysis of diversity and spatial multiplexing schemes both with and without channel state information at the transmitter. In the diversity scheme, our results

show there is little to be gained in terms of energy efficiency at the transmitter by increasing the number of transmit antennas, as long as $N_{\mathrm{r}} \geq 4$ at the base station. Without a known CSI at the handset, which is the most common situation in modern wireless communications, additional transmit antennas degrade the energy efficiency. In the MIMO spatial multiplexing scheme, rate increases linearly with the number of transmitter antennas, at the cost of additional handset energy consumption due to the absence of diversity gain. However, the excess number of receive antennas of the case of massive MIMO base station provides the missing diversity gain in the SM scheme, allows to increase bit rate without need to sacrifice the energy efficiency.

Chapter 5

Conclusions

5.1 Research Contributions and Summary

The objective of this work is to develop a comprehensive model to reduce the energy consumption of wireless handset transceiver. In the past, due to the importance of high energy consumption problem, several models have been proposed to capture the energy consumption considering various parameters [6–9, 46]. Through incorporating the strength and the weakness of these models we able to provide an advanced model that covers the remaining gaps by considering limited factors such as: the simplistic of AWGN channel, simple model of class A PA, missing or incorrect PAR of modulation pulse shape, fixed other circuits, short distance of 10 m, missing power control analysis, missing OFDM, missing the impact of massive MIMO. We strive for this accuracy in two ways: 1) we treated the impact of transmitted energy and dissipated energy separately, so the effect of each is clearly understood (see Figure 1.1 for the major milestone development of this work). 2) We modeled the efficiency for various classes of PAs, which have different maximum drain efficiencies and decay rates, as a function of modulation order and transmission distance.

In other words, we modeled the impact of modulation orders and transmission distances, first on the transmitted energy via the formula of probability of error and the formula of propagation loss, respectively. Second, on the dissipated energy via PAR and via the power control, respectively, for classes A and class AB PAs. In this work, we also presented an advanced analysis of energy and spectral efficiency for multiple antennas at the handset by having MIMO and massive MIMO at the base station receiver. Considering that, this analysis uses diversity and spatial multiplexing schemes to measure the impact of having more than one antenna at the handset on the energy consumption and bit rate of that handset. Some other notable conclusions in this work can be stated as:

- Comparing to class A PAs, Class AB PAs can reduce the amount of energy consumption for wireless handsets due to having higher maximum drain efficiency and lower decay rate. In term of linearity, the value PAR for modulation shows that the linearity requirement for high modulation order converges to a value of which class AB PA can handle easily.

- We proved that the roll-off factor of $\alpha = 0.42$ yields the least PAR of modulation pulses, instead of $\alpha = 1$ that is considered in the literature [9], because we used the exact pulse shape in the energy transmit model, which is the square root raised cosine. Considering the roll-off factor of 0.42 can also save bandwidth by about 29%.

- When high power control is in session, for a nearby handset to the base station, OFDM can be used in the uplink scenario without dissipating an extra PA energy at the handset.

- In the diversity scheme, our results show there is little to be gained in terms of energy efficiency at the transmitter by increasing the number of transmitter antennas. Without a known CSI at the handset, additional transmitter antennas results in a degradation for the energy

efficiency. In the MIMO spatial multiplexing scheme, increasing the number of transmitter antennas leads to increase bit rate, at the cost of additional handset energy consumption due to the absence of diversity gain. However, the excess number of receive antennas of the massive MIMO case at the base station provides the missing diversity gain in the SM scheme, which allows to increase bit rate without sacrificing the energy efficiency.

5.2 Areas of Future Work

In the future, there are some directions that can be used to enhance the results of this work. These directions are:

- By considering PA boosting efficiency techniques, such as pre-distortion and Doherty PA the signal processing may increase, but the energy consumption in the wireless handsets will significantly reduce, because higher efficiency leads to dissipate less energy of the PA.

- Considering the impact of techniques such as: channel coding, hybrid automatic repeat request (HARQ), and millimeter wave (mmWave) can be harder to model, but the model will be more realistic results and will be one step closer to the 5G systems, because these technique either is currently used or they are planned to be implemented in the future.

- Considering MIMO to solve the power control issue by spreading the high power level near the base station among multiple handset transmit antennas. This approach can also provide a diversity gain. However, the handset size and the availability of channel state information will be the main constraints for this approach.

- In MIMO systems, considering assumptions other than equal channel gains and equal bit

rates, which yields to varied power back-off levels at PAs, makes the analyses more difficult, yet, closer to the reality.

- Even though the excess number of antennas at the base station in the massive MIMO case provides diversity for the handset, these antennas will be come limited with having multiple users in the system. The other issue in the multiple user model is considering the pilot contamination problem, which will make the analysis harder, yet more mature.

Chapter 6

APPENDICES

6.1 APPENDIX A

For $x = t^2/(Z \cdot \mathrm{SNR})$, Equation (2.10) can be stated as

$$\begin{aligned}
\bar{P}_{e_b} &\leq W \int_0^{\infty} e^{-x} \int_{\sqrt{Z \cdot x \cdot \mathrm{SNR}}}^{\infty} \frac{1}{\sqrt{2\pi}} e^{-t^2/2} dt\, dx \\
&\leq W \int_0^{\infty} \int_0^{t^2/(Z \cdot \mathrm{SNR})} \frac{1}{\sqrt{2\pi}} e^{-t^2/2} e^{-x} dx dt \\
&\leq W \frac{1}{\sqrt{2\pi}} \int_0^{\infty} e^{-t^2/2} (1 - e^{-t^2/(Z \cdot \mathrm{SNR})}) dt \\
&\leq W \cdot \left(\frac{1}{2} - \frac{1}{\sqrt{2\pi}} \int_0^{\infty} (e^{-t^2/2 \cdot (1 + 2/(Z \cdot \mathrm{SNR}))}) dt \right) \\
&\leq W \cdot \left(\frac{1}{2} \cdot \left(1 - \sqrt{\frac{Z \cdot \mathrm{SNR}}{2 + Z \cdot \mathrm{SNR}}} \right) \right)
\end{aligned} \tag{6.1}$$

where $\int_0^{\infty} \frac{1}{\sqrt{2\pi}} e^{-t^2/2} = \mathrm{Q}(0) = 1/2$

6.2 APPENDIX B

$U^{'}(b)$ can be found by taking the first derivative of the right hand side of Eq (2.31) with respect to b as

$$
\begin{aligned}
U^{'}(b) = \; & G(d)\, K_1 \cdot \left(\frac{2^b-1}{b} \cdot (1-\frac{1}{\sqrt{2^b}})(\frac{\sqrt{2^b}+1}{\sqrt{2^b}-1})^{\lambda} \right) + Q \\
& -b\, G(d)\, K_1 \cdot \Bigg(\frac{(2^b-1)(1-\frac{1}{\sqrt{2^b}})(\frac{\sqrt{2^b}+1}{\sqrt{2^b}-1})^{\lambda}}{b^2} + \\
& \qquad \frac{(2^b-1)(\frac{\sqrt{2^b}+1}{\sqrt{2^b}-1})^{\lambda}\log\{2\}}{2b\sqrt{2^b}} + \frac{2^b \cdot (1-\frac{1}{\sqrt{2^b}})(\frac{\sqrt{2^b}+1}{\sqrt{2^b}-1})^{\lambda}\log\{2\}}{b} + \\
& \qquad \frac{\lambda \cdot (2^b-1)(1-\frac{1}{\sqrt{2^b}})\log\{2\}}{b \cdot (\frac{\sqrt{2^b}+1}{\sqrt{2^b}-1})^{1-\lambda}} \cdot \left(\frac{2^b \cdot \log\{2\}}{2 \cdot (\sqrt{2^b}+1)} - \frac{2^b \cdot (2^b-1)\log\{2\}}{2 \cdot (\sqrt{2^b}+1)^2} \right) \Bigg).
\end{aligned}
\tag{6.2}
$$

Then, this can be simplified as

$$
\begin{aligned}
= Q - \; & G(d)\, K_1 \log\{2\} \cdot \Bigg(\frac{(2^b-1)(\frac{\sqrt{2^b}+1}{\sqrt{2^b}-1})^{\lambda}}{2\sqrt{2^b}} + 2^b \cdot (1-\frac{1}{\sqrt{2^b}})(\frac{\sqrt{2^b}+1}{\sqrt{2^b}-1})^{\lambda} + \\
& \qquad \left(\sqrt{2^b} - 2^b + 2\right) \cdot \frac{\lambda \cdot (2^b-1)\sqrt{2^b} \cdot (\sqrt{2^b}-1)^{2-\lambda}\log\{2\}}{2 \cdot (\sqrt{2^b}+1)^{3-\lambda}} \Bigg).
\end{aligned}
\tag{6.3}
$$

6.3 APPENDIX C

The second derivative of $U(b)$ with respect to b, $U^{''}(b)$, is obtained by differentiating Eq. (6.3), yielding

$$U^{''}(b) = -\,G(d)\,K_1 \cdot \log\{2\}\,\frac{d}{db}\left(\frac{(2^b-1)(\frac{\sqrt{2^b}+1}{\sqrt{2^b}-1})^{\lambda}}{2\sqrt{2^b}} + 2^b \cdot (1-\frac{1}{\sqrt{2^b}})(\frac{\sqrt{2^b}+1}{\sqrt{2^b}-1})^{\lambda} + \right.$$
$$\left. \left(\sqrt{2^b}-2^b+2\right) \cdot \frac{\lambda \cdot (2^b-1)\sqrt{2^b} \cdot (\sqrt{2^b}-1)^{2-\lambda}\log\{2\}}{2 \cdot (\sqrt{2^b}+1)^{3-\lambda}} \right) < 0, \tag{6.4}$$

which clearly shows that $U(b)$ is a concave function.

6.4 APPENDIX D

Starting from (4.5), and with using the Chi-squared function we can have

$$\begin{aligned}
\bar{p}_{eb} \leq & W \;\; \mathbb{E}_h \left\{ Q\left(\sqrt{Z \cdot \mathrm{SNR} \sum_{l=1}^{N_\mathrm{r}} |h_l|^2} \right) \right\} \\
\leq & W \int_0^\infty Q\left(\sqrt{Z \cdot \mathrm{SNR}\, x} \right) f(x) dx \\
\leq & W \int_0^\infty \frac{x^{N_\mathrm{r}-1}}{(N_\mathrm{r}-1)!} e^{-x} \int_{\sqrt{Z \cdot \mathrm{SNR}\, x}}^\infty \frac{1}{\sqrt{2\pi}} e^{-t^2/2} dt dx \\
\leq & W \int_0^\infty \int_0^{t^2/(Z \cdot \mathrm{SNR})} \frac{1}{\sqrt{2\pi}} e^{-t^2/2} \frac{x^{N_\mathrm{r}-1}}{(N_\mathrm{r}-1)!} e^{-x} dx dt \\
\leq & W \int_0^\infty \frac{1}{\sqrt{2\pi}} e^{-t^2/2} \cdot \left(\int_0^{t^2/(Z \cdot \mathrm{SNR})} \frac{x^{N_\mathrm{r}-1}}{(N_\mathrm{r}-1)!} e^{-x} dx \right) dt.
\end{aligned} \tag{6.5}$$

The term in the square brackets above is the cumulative distribution function (CDF) of the gamma distribution, which, according to [91, Sec. 3.3], is related to the Poisson distribution as :

$$\int_0^{t^2/(Z \cdot \mathrm{SNR})} \frac{x^{N_\mathrm{r}-1}}{(N_\mathrm{r}-1)!} e^{-x} dx \quad = \quad 1 - \sum_{l=0}^{N_\mathrm{r}-1} \frac{e^{-t^2/(Z \cdot \mathrm{SNR})}}{l!} \cdot \Big(\frac{t^2}{Z \cdot \mathrm{SNR}} \Big)^l. \tag{6.6}$$

Then:

$$\bar{P}_{e_b} \leq W \int_0^\infty \frac{1}{\sqrt{2\pi}} e^{-t^2/2} \cdot \left(1 - \sum_{l=0}^{N_\mathrm{r}-1} \frac{e^{-t^2/(Z \cdot \mathrm{SNR})}}{l!} \cdot \Big(\frac{t^2}{Z \cdot \mathrm{SNR}} \Big)^l \right) dt \tag{6.7}$$

This formula is the even moments of the standard Gaussian distribution [92, Sec. 3.5] which can

be resolved as

$$\bar{P}_{e_b} \leq W \cdot \left(\frac{1-\mu}{2}\right)^{N_\mathrm{r}} \cdot \sum_{l=0}^{N_\mathrm{r}-1} \binom{N_\mathrm{r}-1+l}{l} \left(\frac{1+\mu}{2}\right)^{l}. \tag{6.8}$$

6.5 Abbreviations

Table 6.1: List of Abbreviations

Abbreviation	Description
3G	The Third generation wireless communication systems
4G	The Fourth generation wireless communication systems
5G	The Fifth generation wireless communication systems
AWGN	Additive white Gaussian noise
ADC	Analog-to-digital converter
BW	Bandwidth
CMOS	Complementary metal oxide semiconductor
CPU	Central processing unit
CSI	Channel state information
CSIR	Channel state information at receiver
CSIT+R	Channel state information at the transmitter and receiver
DAC	Digital-to-analog converter
dBmJ	Decibels relative to a millijoule
i.i.d	Independent and identically distributed
ISI	Inter-Symbol Interference)
LNA	Low-noise-amplifier
LO	Local oscillator

Abbreviation	Description
MIMO	Multiple-input-multiple-output
MMSE	Minimum mean squared error
MOD	Modulation
MQAM	Multilevel quadrature amplitude modulation
MRC	Maximal ratio combining
MSB	Most significant bit
NOMA	Non-orthogonal multiple access
LSB	Least significant bit
OFDM	Orthogonal frequency division multiplexing
PA	Power amplifier
PAD	Power amplifier dissipated
PAR	Peak to average power ratio
PBSK	Binary phase shift keying
QPSK	Quadratic phase shift keying
RC	Raised-cosine
RF	Radio frequency
SC	Selection combining
SM	Spatial multiplexing
SISO	Single-input-single-output
SNR	Signal to noise ratio
SRRC	Square-root-raised cosine pulses
VBLAST	Vertical Bell laboratories layered space-time
ZF	Zero forcing

6.6 Mathematical Notations

Table 6.2: List of Mathematical Notations

Notation	Description
$a!$	Factorial of a
$a(t)$	Continuous function $a(t)$ dependent on variable t
$a \cdot (t)$	a multiplied by (t); used to identify multiplication from function as using parenthesis
$\max\{a, t\}$	Choose the maximum of a and t
$\max_i(a_i)$	maximum of a over variable i
$\mathbb{E}\{a\}$	Expected value of a
$\lceil a \rceil$	denotes the smallest integer greater than or equal to a
a^*	The optimum value of a as a result of the optimization
$a \approx t$	a is approximate to t
$a = t$	a is equal to t
$a \sim D$	The random variable a has the probability distribution D
$a \in \text{odd}(\mathbb{N})$	a is odd integer
$a \in \text{even}(\mathbb{N})$	a is even integer
$a \in \mathbb{N}$	a is integer
$\lvert a \rvert$	Magnitude of a
$D'(a)$	First derivative of D with respect to a

Notation	Description
$D''(a)$	Second derivative of D with respect to a
$\frac{\partial}{\partial a}(D)$	Partial derivative of D with respect to a
$\{a, t\}$	Set containing a and t
$\bar{a}$	average value of a
$\mathrm{Q}(\cdot)$	The Gaussian Q-function
$a \leq t$	a is larger or equal to t
$a < t$	a is smaller than t
$\binom{a}{t}$	is binomial coefficient with a success in a sequence of t trials
$\underset{t}{\text{maximize}}\ a(t)$	Maximum of $a(t)$ over variable t
$\log\{a\}$	log for a with the base of e
$\log_{10}\{a\}$	log for a with the base of 10
$\log_2\{a\}$	log for a with the base of 2
a in dB	a in decibels = $10\log_{10}\{a\}$

References

[1] G. Auer, V. Giannini, C. Desset, I. Godor, P. Skillermark, M. Olsson, M. A. Imran, D. Sabella, M. J. Gonzalez, O. Blume *et al.*, "How much energy is needed to run a wireless network?" *Wireless Communications, IEEE*, vol. 18, no. 5, pp. 40–49, 2011.

[2] F. Tan and S. Fok, "Thermal management of mobile phone using phase change material," in *Electronics Packaging Technology Conference, 2007. EPTC 2007. 9th*. IEEE, 2007, pp. 836–842.

[3] A. Carroll and G. Heiser, "An analysis of power consumption in a smartphone." in *USENIX annual technical conference*, 2010, pp. 271–285.

[4] D. Feng, C. Jiang, G. Lim, L. J. Cimini, G. Feng, and G. Y. Li, "A survey of energy-efficient wireless communications," *IEEE Communications Surveys & Tutorials*, vol. 15, no. 1, pp. 167–178, 2013.

[5] A. Gupta and R. K. Jha, "A survey of 5G network: Architecture and emerging technologies," *IEEE access*, vol. 3, pp. 1206–1232, 2015.

[6] S. Cui, A. J. Goldsmith, and A. Bahai, "Energy-constrained modulation optimization," *Wireless Communications, IEEE Transactions on*, vol. 4, no. 5, pp. 2349–2360, 2005.

[7] ——, "Modulation optimization under energy constraints," in *Communications, 2003. ICC'03. IEEE International Conference on*, vol. 4. IEEE, 2003, pp. 2805–2811.

[8] Y. Li, B. Bakkaloglu, and C. Chakrabarti, "A system level energy model and energy-quality evaluation for integrated transceiver front-ends," *Very Large Scale Integration (VLSI) Systems, IEEE Transactions on*, vol. 15, no. 1, pp. 90–103, 2007.

[9] ——, "A comprehensive energy model and energy-quality evaluation of wireless transceiver front-ends," in *IEEE Workshop on Signal Processing Systems Design and Implementation, 2005.* IEEE, 2005, pp. 262–267.

[10] G. Miao, N. Himayat, and G. Y. Li, "Energy-efficient link adaptation in frequency-selective channels," *Communications, IEEE Transactions on*, vol. 58, no. 2, pp. 545–554, 2010.

[11] C. Schurgers, O. Aberthorne, and M. Srivastava, "Modulation scaling for energy aware communication systems," in *the international symposium on Low power electronics and design*. ACM, 2001.

[12] J. Joung, C. K. Ho, K. Adachi, and S. Sun, "A survey on Power-Amplifier-centric techniques for spectrum-and energy-efficient wireless communications," *Communications Surveys & Tutorials, IEEE*, vol. 17, no. 1, pp. 315–333, 2015.

[13] F. Rosas and C. Oberli, "Modulation and snr optimization for achieving energy-efficient communications over short-range fading channels," *IEEE Transactions on Wireless Communications*, vol. 11, no. 12, pp. 4286–4295, 2012.

[14] T. S. Rappaport *et al.*, *Wireless communications: principles and practice*, 1996, vol. 2.

[15] L. Zhu, J. Zhang, Z. Xiao, X. Cao, D. O. Wu, and X.-G. Xia, "Joint power control and beamforming for uplink non-orthogonal multiple access in 5g millimeter-wave communications," *IEEE Transactions on Wireless Communications*, vol. 17, no. 9, pp. 6177–6189, 2018.

[16] Y. Saito, Y. Kishiyama, A. Benjebbour, T. Nakamura, A. Li, and K. Higuchi, "Non-orthogonal multiple access (noma) for cellular future radio access," in *Vehicular Technology Conference (VTC Spring), 2013 IEEE 77th*. IEEE, 2013, pp. 1–5.

[17] N. Zhang, J. Wang, G. Kang, and Y. Liu, "Uplink nonorthogonal multiple access in 5g systems," *IEEE Communications Letters*, vol. 20, no. 3, pp. 458–461, March 2016.

[18] H. Q. Ngo, A. Ashikhmin, H. Yang, E. G. Larsson, and T. L. Marzetta, "Cell-free massive MIMO versus small cells," *IEEE Transactions on Wireless Communications*, vol. 16, no. 3, pp. 1834–1850, 2017.

[19] T. C. Mai, H. Q. Ngo, M. Egan, and T. Q. Duong, "Pilot power control for cell-free massive mimo," *IEEE Transactions on Vehicular Technology*, vol. 67, no. 11, pp. 11 264–11 268, Nov 2018.

[20] J. Proakis and M. Salehi, *Digital Communications*, 5th ed. New York: McGraw-Hill, 2007.

[21] F. Mahmood, E. Perrins, and L. Liu, "Modeling and analysis of energy consumption for RF transceivers in wireless cellular systems," in *2015 IEEE Global Communications Conference (GLOBECOM)*. IEEE, 2015, pp. 1–6.

[22] F. E. Mahmood, E. S. Perrins, and L. Liu, "Modeling and analysis of energy consumption for MIMO systems," in *Wireless Communications and Networking Conference (WCNC), 2017 IEEE*. IEEE, 2017, pp. 1–6.

[23] F. Mahmood, E. Perrins, and L. Liu, "Modeling and analysis of power amplifier dissipation energy in wireless handset transceivers," in *2018 International Conference on Computing, Networking and Communications (ICNC)*. IEEE, 2018, pp. 1–6.

[24] F. E. Mahmood, E. S. Perrins, and L. Liu, "Energy consumption vs. bit rate analysis toward massive mimo systems," in *2018 IEEE International Smart Cities Conference (ISC2)*. IEEE, 2018, pp. 1–7.

[25] L. Liu, G. Miao, and J. Zhang, "Energy-efficient scheduling for downlink multi-user MIMO," in *Communications (ICC), 2012 IEEE International Conference on*. IEEE, 2012, pp. 4394–4394.

[26] X. Ge, X. Huang, Y. Wang, M. Chen, Q. Li, T. Han, and C.-X. Wang, "Energy-efficiency optimization for MIMO-OFDM mobile multimedia communication systems with QoS constraints," *Vehicular Technology, IEEE Transactions on*, vol. 63, no. 5, pp. 2127–2138, 2014.

[27] K. K. Mensah, R. Chai, D. Bilibashi, and F. Gao, "Energy efficiency based joint cell selection and power allocation scheme for HetNets," *Digital Communications and Networks*, vol. 2, no. 4, pp. 184 – 190, 2016.

[28] A. C. Cirik, S. Biswas, S. Vuppala, and T. Ratnarajah, "Beamforming design for full-duplex MIMO interference channels–QoS and Energy-Efficiency considerations," *IEEE Transactions on Communications*, vol. 64, no. 11, pp. 4635–4651, 2016.

[29] A. Puglielli, A. Townley, G. LaCaille, V. Milovanović, P. Lu, K. Trotskovsky, A. Whitcombe, N. Narevsky, G. Wright, T. Courtade *et al.*, "Design of Energy-and Cost-Efficient Massive MIMO Arrays," *Proceedings of the IEEE*, vol. 104, no. 3, pp. 586–606, 2016.

[30] L. Zheng and D. N. Tse, "Diversity and multiplexing: a fundamental tradeoff in multiple-antenna channels," *Information Theory, IEEE Transactions on*, vol. 49, no. 5, pp. 1073–1096, 2003.

[31] F. Rosas and C. Oberli, "Impact of the Channel State Information on the Energy-Efficiency of MIMO communications," *IEEE Transactions on Wireless Communications*, vol. 14, no. 8, pp. 4156–4169, Aug 2015.

[32] R. Cavalcante, S. Stanczak, M. Schubert, A. Eisenblaetter, and U. Turke, "Toward energy-efficient 5G wireless communications technologies," *Signal Processing Magazine, IEEE*, vol. 31, no. 6, pp. 24–34, 2014.

[33] A. Waheed and A. Ashik, "Mitigation of phase noise at millimeter-wave frequencies for wireless personal area network applications," *Masters Theses*, p. 180, 2008.

[34] F. H. Raab, P. Asbeck, S. Cripps, P. B. Kenington, Z. B. Popovic, N. Pothecary, J. F. Sevic, and N. O. Sokal, "Power amplifiers and transmitters for RF and microwave," *Microwave Theory and Techniques, IEEE Transactions on*, vol. 50, no. 3, pp. 814–826, 2002.

[35] S. Jorgensen, "Modelling of power dissipation in CMOS DACs," 2002.

[36] J. Wu, G. Wang, and Y. R. Zheng, "Energy efficiency and spectral efficiency tradeoff in type-I ARQ systems," *IEEE Journal on Selected Areas in Communications*, vol. 32, no. 2, pp. 356–366, 2014.

[37] I. Pehlivan and S. C. Ergen, "Scheduling of energy harvesting for mimo wireless powered communication networks," *IEEE Communications Letters*, vol. 23, no. 1, pp. 152–155, 2019.

[38] Y. Zeng, J. Xu, and R. Zhang, "Energy minimization for wireless communication with rotary-wing uav," *IEEE Transactions on Wireless Communications*, 2019.

[39] K. Wang, K. Yang, and C. S. Magurawalage, "Joint energy minimization and resource allocation in c-ran with mobile cloud," *IEEE Transactions on Cloud Computing*, vol. 6, no. 3, pp. 760–770, 2018.

[40] A. Samanta and S. Misra, "Energy-efficient and distributed network management cost minimization in opportunistic wireless body area networks," *IEEE Transactions on Mobile Computing*, vol. 17, no. 2, pp. 376–389, 2018.

[41] Q. Yao, A. Huang, H. Shan, and T. Q. Quek, "Wet-enabled passive communication networks: Robust energy minimization with uncertain csi distribution," *IEEE Transactions on Wireless Communications*, vol. 17, no. 1, pp. 282–295, 2018.

[42] T. Van Chien, E. Björnson, and E. G. Larsson, "Joint power allocation and user association optimization for massive mimo systems," *IEEE Transactions on Wireless Communications*, vol. 15, no. 9, pp. 6384–6399, 2016.

[43] S. C. Cripps, *RF power amplifiers for wireless communications*, 2nd ed. Artech House, Inc., 2006.

[44] A. anadigics inc., *ALT5020 High Efficiency UMTS E800 LTE Linear*, New Jersey, 2013. [Online]. Available: http://www.anadigics.com

[45] D. Tse and P. Viswanath, *Fundamentals of wireless communication*. Cambridge university press, 2005.

[46] S. Cui, A. J. Goldsmith, and A. Bahai, "Energy-efficiency of MIMO and cooperative MIMO techniques in sensor networks," *Selected Areas in Communications, IEEE Journal on*, vol. 22, no. 6, pp. 1089–1098, 2004.

[47] Z.-Q. Luo and J.-S. Pang, "Analysis of iterative waterfilling algorithm for multiuser power control in digital subscriber lines," *EURASIP Journal on Advances in Signal Processing*, vol. 2006, no. 1, p. 024012, 2006.

[48] M. Gustavsson, J. J. Wikner, and N. Tan, *CMOS data converters for communications*. Springer, 2000.

[49] K. Cho and D. Yoon, "On the general ber expression of one-and two-dimensional amplitude modulations," *IEEE Transactions on Communications*, vol. 50, no. 7, pp. 1074–1080, 2002.

[50] A. Conti, M. Z. Win, and M. Chiani, "Invertible bounds for M-QAM in Rayleigh fading," *IEEE Transactions on Wireless Communications*, vol. 4, no. 5, pp. 1994–2000, 2005.

[51] A. Goldsmith, *Wireless communications*. Cambridge university press, 2005.

[52] T. Starr, J. M. Cioffi, and P. J. Silverman, *Understanding digital subscriber line technology*. Prentice Hall PTR, 1999.

[53] S. Verdu, "On channel capacity per unit cost," *IEEE Transactions on Information Theory*, vol. 36, no. 5, pp. 1019–1030, 1990.

[54] A. Y. Wang and C. G. Sodini, "On the energy efficiency of wireless transceivers," in *Communications, 2006. ICC'06. IEEE International Conference on*, vol. 8. IEEE, 2006, pp. 3783–3788.

[55] M. Ji, D. Teeter, S. Richard, E. Shull, and D. Mahoney, "Envelope tracking power amplifier design considerations for handset applications," in *2016 IEEE Topical Conference on Power Amplifiers for Wireless and Radio Applications (PAWR)*, Jan 2016, pp. 27–29.

[56] B. Berglund, J. Johansson, and T. Lejon, "High efficiency power amplifiers," *Ericsson Review*, vol. 83, no. 3, pp. 92–96, 2006.

[57] F. Raab, "Efficiency of outphasing RF power-amplifier systems," *IEEE Transactions on Communications*, vol. 33, no. 10, pp. 1094–1099, 1985.

[58] P. B. Kenington, *High linearity RF amplifier design*. Artech House, Inc., 2000.

[59] S. W. Amos and M. James, *Principles of transistor circuits*. London: Butterworths, 1984.

[60] S. L. Miller and R. J. O'Dea, "Peak power and bandwidth efficient linear modulation," *Communications, IEEE Transactions on*, vol. 46, no. 12, pp. 1639–1648, 1998.

[61] X. Zhang, L. E. Larson, and P. Asbeck, *Design of linear RF outphasing power amplifiers*. Artech House, 2003.

[62] H. Ochiai, "An analysis of band-limited communication systems from amplifier efficiency and distortion perspective," *IEEE Transactions on Communications*, vol. 61, no. 4, pp. 1460–1472, 2013.

[63] J. Jeong, D. F. Kimball, M. Kwak, P. Draxler, and P. M. Asbeck, "Envelope tracking power amplifiers with reduced peak-to-average power ratio rf input signals," in *Radio and Wireless Symposium (RWS), 2010 IEEE*. IEEE, 2010, pp. 112–115.

[64] P. Colantonio, F. Giannini, R. Giofrè, and L. Piazzon, "The AB-C Doherty power amplifier. part i: Theory," *International Journal of RF and Microwave Computer-Aided Engineering*, vol. 19, no. 3, pp. 293–306, 2009.

[65] J. C. Pedro, N. B. Carvalho, C. Fager, and J. A. Garcia, "Linearity versus efficiency in mobile handset power amplifiers: A battle without a loser," *Microwave Engineering Europe (August 2004)*, 2004.

[66] S. P. Stapleton and A. E. EDA, "Digital predistortion of power amplifiers," *Agilent Technol. Inc., Santa Clara, CA*, 2005.

[67] J. Li, X.-D. Zhang, Q. Gao, Y. Luo, and D. Gu, "Exact BEP analysis for coherent M-ary PAM and QAM over AWGN and Rayleigh fading channels," in *Vehicular Technology Conference, 2008. VTC Spring 2008. IEEE*. IEEE, 2008, pp. 390–394.

[68] S. Daumont, B. Rihawi, and Y. Lout, "Root-raised cosine filter influences on PAPR distribution of single carrier signals," in *Communications, Control and Signal Processing, 2008. ISCCSP 2008. 3rd International Symposium on*. IEEE, 2008, pp. 841–845.

[69] D. Kim, D. Kang, J. Choi, J. Kim, Y. Cho, and B. Kim, "Optimization for envelope shaped operation of envelope tracking power amplifier," *IEEE transactions on microwave theory and techniques*, vol. 59, no. 7, pp. 1787–1795, 2011.

[70] M. Hassan, L. E. Larson, V. W. Leung, and P. M. Asbeck, "A combined series-parallel hybrid envelope amplifier for envelope tracking mobile terminal rf power amplifier applications," *IEEE Journal of Solid-State Circuits*, vol. 47, no. 5, pp. 1185–1198, 2012.

[71] M. Hassan, L. E. Larson, V. W. Leung, D. F. Kimball, and P. M. Asbeck, "A wideband CMOS/GaAs HBT envelope tracking power amplifier for 4g lte mobile terminal applications," *IEEE Transactions on Microwave Theory and Techniques*, vol. 60, no. 5, pp. 1321–1330, 2012.

[72] J. Choi, D. Kim, D. Kang, and B. Kim, "A new power management IC architecture for envelope tracking power amplifier," *IEEE Transactions on Microwave Theory and Techniques*, vol. 59, no. 7, pp. 1796–1802, 2011.

[73] T. Jiang and Y. Wu, "An overview: peak-to-average power ratio reduction techniques for OFDM signals," *IEEE transactions on broadcasting*, vol. 54, no. 2, pp. 257–268, 2008.

[74] S. R. Herlekar, C. Zhang, H.-C. Wu, A. Srivastava, and Y. Wu, "OFDM performance analysis in the phase noise arising from the hot-carrier effect," *Consumer Electronics, IEEE Transactions on*, vol. 52, no. 3, pp. 757–765, 2006.

[75] Q. Gu, *RF system design of transceivers for wireless communications*. Springer Science & Business Media, 2005.

[76] S. Soliman, C. Wheatley, and R. Padovani, "Cdma reverse link open loop power control," in *Global Telecommunications Conference, 1992. Conference Record., GLOBECOM'92. Communication for Global Users., IEEE*. IEEE, 1992, pp. 69–73.

[77] T. S. Rappaport, S. Sun, R. Mayzus, H. Zhao, Y. Azar, K. Wang, G. N. Wong, J. K. Schulz, M. Samimi, and F. Gutierrez, "Millimeter wave mobile communications for 5G cellular: It will work!" *Access, IEEE*, vol. 1, pp. 335–349, 2013.

[78] B. Flores-Centurion, "The peak factor of a 16-QAM/ OFDM system," 2007.

[79] T. L. Marzetta, "Massive MIMO: an introduction," *Bell Labs Technical Journal*, vol. 20, pp. 11–22, 2015.

[80] H. Q. Ngo, E. G. Larsson, and T. L. Marzetta, "Energy and spectral efficiency of very large multiuser MIMO systems," *IEEE Transactions on Communications*, vol. 61, no. 4, pp. 1436–1449, 2013.

[81] E. Bjørnson, J. Hoydis, M. Kountouris, and M. Debbah, "Massive MIMO systems with non-ideal hardware: Energy efficiency, estimation, and capacity limits," *IEEE Transactions on Information Theory*, vol. 60, no. 11, pp. 7112–7139, 2014.

[82] D. Seethaler, H. Artes, and F. Hlawatsch, "Detection techniques for MIMO spatial multiplexing systems," *e&i Elektrotechnik und Informationstechnik*, vol. 122, no. 3, pp. 91–96, 2005.

[83] L. Ordoez, D. P. Palomar, J. R. Fonollosa *et al.*, "High-SNR analytical performance of spatial multiplexing MIMO systems with CSI," *Signal Processing, IEEE Transactions on*, vol. 55, no. 11, pp. 5447–5463, 2007.

[84] E. Basar, M. Wen, R. Mesleh, M. Di Renzo, Y. Xiao, and H. Haas, "Index modulation techniques for next-generation wireless networks," *IEEE Access*, vol. 5, pp. 16 693–16 746, 2017.

[85] H. Ren, N. Liu, C. Pan, and C. He, "Energy efficiency optimization for MIMO distributed antenna systems," *IEEE Transactions on Vehicular Technology*, vol. 66, no. 3, pp. 2276–2288, 2017.

[86] M. K. Simon and M.-S. Alouini, *Digital communication over fading channels*. John Wiley & Sons, 2005, vol. 95.

[87] S. M. Alamouti, "A simple transmit diversity technique for wireless communications," *Selected Areas in Communications, IEEE Journal on*, vol. 16, no. 8, pp. 1451–1458, 1998.

[88] H. Jafarkhani, *Space-time coding: theory and practice*. Cambridge university press, 2005.

[89] S. Verdú, "Computational complexity of optimum multiuser detection," *Algorithmica*, vol. 4, no. 1, pp. 303–312, 1989.

[90] J. R. Hampton, *Introduction to MIMO communications*. Cambridge university press, 2013.

[91] R. V. Hogg and A. T. Craig, *Introduction to Mathematical Statistics: 3d Ed.* Macmillan, 1970.

[92] J. B. Walsh, *Knowing the odds: an introduction to probability*. American Mathematical Soc., 2012, vol. 139.